Designing Time-Hopping Ultra-Wide Bandwidth Receivers for Multi-User Interference Environments

Norman C. Beaulieu and David J. Young

***Abstract*—The multiple-user interference (MUI) in time-hopped impulse-radio ultra-wide bandwidth (UWB) systems is impulse-like and poorly approximated by a Gaussian distribution. Therefore, conventional matched filter receiver designs, which are optimal for Gaussian noise, are not fully efficient for UWB applications. Several alternative distributions for approximating the MUI process and the MUI-plus-noise process in UWB systems are motivated and compared. These distributions have in common that they are more impulsive than the Gaussian approximation, with a greater area in the tails of the probability density function (pdf) compared to a Gaussian pdf. The improved MUI and MUI-plus-noise models are utilized to derive new receiver designs for UWB applications, which are shown to be superior to the conventional matched filter receiver.**

Multipath propagation is abundant in UWB channels and is exploited by a Rake receiver. A Rake receiver uses multiple fingers to comb the multipath rays with a conventional matched filter implemented in each finger. Rake structures utilizing the new receiver designs that are suitable for reception of UWB signals in multipath fading channels are provided. An optimal performance benchmark, based on an accurate theoretical model for the interference which fully explains the features of the MUI pdf, is also presented. Analysis and simulation results are shown for the novel receivers which demonstrate that the new designs have superior performance compared to the conventional linear receiver when MUI is significant. Several adaptive receivers are shown to always match or exceed the performance of the conventional linear receiver in all MUI-plus-noise environments. Parameter estimation for the new receivers also is discussed.

***Index Terms*—Demodulation, digital receivers, error rate, multiple-access interference (MAI), multiuser interference (MUI), Rake receiver, receiver design, ultra-wide bandwidth (UWB).**

I. Introduction

Ultra-wide bandwidth (UWB) wireless communication systems have seen growing research interest and industrial activity. While UWB signaling has been used for radar and location purposes for over 20 years, the appeal of UWB signaling for communications has been more recent. Several key features make UWB attractive for a number of timely applications. Extremely low transmitted power allows for UWB signals to underlay other users of the same radio spectrum; the United States Federal Communications Commission (FCC) has established spectral masks for operation of UWB systems, allowing unlicensed UWB systems to underlay licensed users in the same frequency spectrum [1], and similar conventions have occurred around the world [2]. The FCC spectral masks, specified separately for indoor and outdoor applications, are designed such that UWB transmissions do not cause interference with existing narrowband users; rather, the ultra-wide bandwidth and ultra-low power signals are below the receiver noise floor in licensed spectral regions. Thus, UWB signaling makes a wide bandwidth available for unlicensed uses, bandwidth that might otherwise go unused at a particular time and point in space. As wireless devices become even more prevalent, the need for simultaneous, collocated frequency reuse, such as offered by UWB systems, becomes paramount. Proposed applications for UWB systems include wireless personal-area networks, short-range high-rate communication between consumer electronics and computer devices in the home, home automation, sensor networks, etc. The short UWB pulse also embodies position location and ranging capability within the modulation itself, allowing small, low-cost devices to be equipped with positioning features and further increasing the variety of imaginable applications. As well, the propagation characteristics of UWB signals allow for a high degree of spatial frequency reuse, important as an increasing number of devices are equipped with wireless features and as wireless connectivity becomes a key consumer expectation.

Proposed UWB systems can be divided into two broad classes, those based on a multi-band approach such as orthogonal frequency-division multiplexing (OFDM), and those based on impulse radio (IR). IR systems [3]-[5] use an ultra-short signaling pulse transmitted at baseband, with no explicit modulation/demodulation components required in the transmitter or receiver. IR-UWB systems can be further divided into systems which use direct-sequence (DS) codes (DS-UWB) and systems which use time-hopping (TH) codes (TH-UWB). The focus of this article is communication using time-hopped impulse radio in the presence of interfering TH-UWB users. It is critical to distinguish between the types of UWB systems when considering multiple-user interference (MUI).[1] Time-hopped systems, which will be described in more detail below, have substantially different MUI characteristics than DS-UWB or UWB-OFDM systems and demand different MUI models for use in system analysis and design; the almost ubiquitous Gaussian interference model which has been used extensively for a variety of communication systems is generally not an accurate model for the MUI in TH-UWB communications, as will be demonstrated. An overview of several superior receivers designed with reference to accurate MUI models will be given. Moreover, Gaussian noise is a significant impairment in addition to MUI, and both the signal-to-noise ratio (SNR) and the signal-to-interference ratio (SIR) will be relevant to system performance. An effective UWB receiver must work well in the continuum between the low-SNR–high-SIR regime,

[1]The term *multiple-access interference* (MAI) is used interchangably with the term *multiple-user interference* (MUI) in the UWB literature. We will use the latter term.

which will have Gaussian noise as a dominant impairment, and the high-SNR–low-SIR regime, which will be dominated by non-Gaussian interference. The receivers discussed here include adaptive implementations that provide excellent or optimal performance in this continuum.

UWB systems also experience interference from narrowband systems. Modeling and mitigation of narrowband interference is not considered in this paper but is considered in many other works (see, for example, [6]-[9]).

The remainder of this paper is structured as follows. Section II gives a brief overview of TH-UWB systems and other relevant aspects of UWB communications, such as UWB channel models. Section III considers MUI in depth, recalling the salient features of MUI in TH-UWB systems, and motivating and evaluating several MUI models. Section IV discusses several proposed receivers that achieve superior performance in channel conditions where MUI is a dominant impairment. The receivers are presented first for an additive white Gaussian noise (AWGN) channel for clarity, with detection in multipath channels covered in Section V. Section VI considers practical estimation of the operating parameters required in each receiver design. A conclusion and summary can be found in Section VII.

II. Time-Hopped UWB Systems

A. The UWB Signal Format

Time-hopped UWB systems [3]-[5] use a very short basic signaling pulse which will be denoted $p(t)$. For purposes of analysis, the pulse may be considered to be normalized to unit energy, i.e. $\int_{-\infty}^{\infty} p^2(t)dt = 1$ and to have pulse width T_p, where T_p is typically less than 1 ns. Fundamental to time-hopped UWB systems is a frame structure with frames of length T_f divided into chip slots of width T_c (Fig. 1). A given source data bit is repeatedly transmitted over a number of frames, N_s, in effect forming a length-N_s repetition code [3]-[5], [10]. The repetition code allows reliable decisions to be made while the energy per transmitted pulse (chip) can be made very small, a property essential for underlaying other radio systems. In each frame, the transmitted pulse is shifted to a different chip slot by a hopping code $\{c_i^{(k)}\}$, where i is the frame index, k is the user index, and $c_i^{(k)} \in \{0, 1 \ldots, N_h - 1\}$. Each user's hopping code is unique, and the use of the hopping codes avoids the situation where the signals from multiple users overlap entirely and every chip associated with a given data symbol experiences a collision with a signal chip from another user. Rather, when a chip collision occurs, adjacent frames associated with the same transmitted symbols and the same users will probably not also experience a collision. Each user signal in a TH-UWB system has low duty cycle; i.e, the frame duration T_f is much larger than T_c and T_p, and the symbol duration is $T_b = N_s T_f$.

For most of this paper, we will consider a time-hopped binary phase-shift keying (TH-BPSK) UWB system, in which the sign of the basic pulse $p(t)$ is modulated according to the data bit. Also common are time-hopped pulse-position modulation (TH-PPM) UWB systems, in which the basic pulse $p(t)$ is time-shifted for, say, a source bit of 1, with no time shift applied for a source bit of 0. The results of this paper are readily extended to TH-PPM systems. The signal pictured in Fig. 1 uses TH-BPSK modulation.

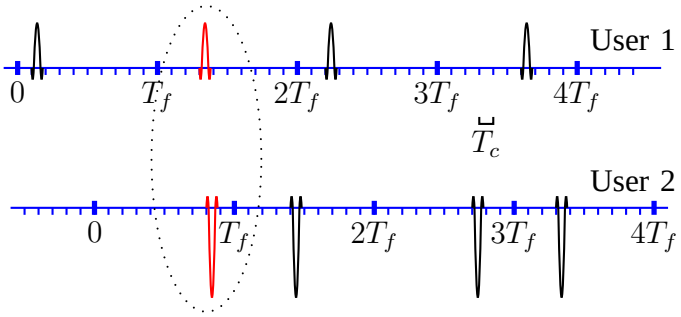

Fig. 1. The frame structure of two asynchronous TH-BPSK signals. The repeated pulses in each user signal are employed to transmit the same data symbol. The pulses in red have experienced a collision; the time-hopping code ensures that other frames associated with the same data symbols rarely also experience a collision.

The most commonly reported pulse $p(t)$ for studies of TH-UWB systems is the second-order Gaussian monocycle,

$$p(t) = \frac{4}{\sqrt{6T_m}} \exp\left[-2\pi \frac{t}{T_m}^2\right] \left[1 - 4\pi \left(\frac{t}{T_m}\right)^2\right] \quad (1)$$

where $p(t)$ has been normalized to unit energy, and T_m is a parameter controlling the pulse width. Families of more practical time-limited UWB pulses are proposed in [11].

With energy per bit E_b, the transmitted TH-BPSK signal for the kth user can be written as

$$s^{(k)}(t) = \sqrt{\frac{E_b}{N_s}} \sum_{i=-\infty}^{\infty} d^{(k)}_{\lfloor i/N_s \rfloor} p\left(t - iT_f - c_i^{(k)} T_c\right) \quad (2)$$

where $\lfloor x \rfloor$ represents the nearest integer less than or equal to x and $d_j^{(k)}$ is the jth symbol for the kth user. With N_u denoting the number of users in the same coverage area, the received signal in the absence of multipath propagation is

$$r(t) = \sum_{k=1}^{N_u} A_k s^{(k)}(t - \tau_k) + n(t)$$

where A_k is the real-valued channel gain associated with the kth user, and τ_k is the delay of the kth user relative to the desired user 1. The user delays τ_k, $k > 1$ will be modeled as independent and uniformly distributed on $[0, T_b)$; that is, the users transmit asynchronously. Without loss of generality, user 1 is the desired user, with $\tau_1 = 0$, and users $k = 2, \ldots, N_u$ are undesired interfering users. The noise process $n(t)$ is modeled as additive white Gaussian noise (AWGN) with two-sided power spectral density $N_0/2$. The receiver thus must detect the source symbols for user 1 in the background of MUI from users $2, \ldots, N_u$ plus AWGN.

The SIR, based on the output of the conventional correlation receiver, is defined as [3]

$$\text{SIR} = \frac{A_1^2 E_b N_s}{\text{var}\{I\}} \quad (3)$$

where $\mathrm{var}\{I\}$ is the variance of the total interference which can be written as

$$\mathrm{var}\{I\} = \frac{E_b \sum_{k=2}^{N_u} A_k^2}{T_f} \int_{-\infty}^{\infty} \left[\int_{-\infty}^{\infty} p(x-s)p(x)dx \right]^2 ds. \quad (4)$$

Unless otherwise noted, the simulations described in this paper use $T_f = 20$ ns, $T_c = 0.9$ ns, $N_h = 8$, and a second-order Gaussian monocycle pulse with $T_m = 0.2877$ ns.

B. The UWB Channel

Wireless communication systems commonly experience multipath propagation, where multiple paths between transmitter and receiver exist and the received signal is the superposition of signals from all paths. The signal corresponding to each path has a unique time delay and amplitude, which can be represented by a multipath profile of signed-amplitude versus delay. Several useful channel models have been proposed for UWB systems [12]-[15]. The most common reference channel models used for UWB analysis and simulation are those adopted by the IEEE 802.15.3a committee for the evaluation of UWB physical layer proposals [12], summarized in [13]. A key feature of these UWB channel models is that paths are clustered. The clusters arrive according to a Poisson process, and within each cluster the individual rays arrive according to an independent Poisson process of different rate. The gain of a given path is governed by the product of three independent random variables: a lognormal random variable representing cluster fading, an independent lognormal random variable representing the fading of each ray, and a Rademacher-distributed random variable (i.e., ± 1 with equal probability) representing the inversion of the signal due to reflections. There is also overall shadowing represented by an independent lognormal random variable.

The use of lognormal random variables for path gains is in contrast to outdoor land mobile channels, which commonly use a Rayleigh or Ricean distribution. Due to the fine time resolution of the UWB signal, relatively few paths combine at each resolvable channel delay, and the resulting sum is not well-approximated as a Gaussian random variable by the Central Limit Theorem [16].

Parameters for four models, denoted CM1 through CM4 and covering both line-of-sight and non-line-of-sight propagation, were specified by the IEEE 802.15.3a subcommittee and can be found in [13].

III. Analyzing Multiple-User Interference

The focus of this article is TH-UWB communication in MUI, in both single-path and multipath channels. MUI is expected to be a significant impairment in UWB systems because of the wide applicability and expected widespread use of UWB devices, with proposed applications involving several devices co-located in a small area, for example an indoor room or office. The short-range nature of UWB signals suggests a few dominant interferers at close range. This has two consequences. One, the relative signal power of these few dominant interferers may be high. Two, the small number of interferers (coupled with the low duty cycle of the UWB waveform, to be discussed further in the sequel) means that approximation of the interference as a Gaussian process is often inaccurate.[2] Thus, modeling of MUI in TH-UWB systems is a unique and important problem.

A. The Distribution of MUI in TH-UWB

There are a number of contributions in the literature to the modeling of the interference at a TH-UWB receiver generated by other TH-UWB transmitters. In code-division multiple-access (CDMA) systems, MUI can often reasonably be modeled by a Gaussian process, and some authors have extended this assumption to TH-UWB systems. However, there are important differences between CDMA and TH-UWB systems that make the Gaussian assumption inappropriate. Most significantly, a transmitted CDMA signal has a duty cycle that is essentially unity; a pulse is transmitted in every chip slot. When multiple CDMA users are simultaneously transmitting, the receiver sees a superposition of the signals from many independent users in *each* chip slot. The interference process tends to a Gaussian process by the Central Limit Theorem and convergence is relatively fast with respect to the number of users. The Gaussian approximation is convenient in terms of receiver design and analysis since transmission in additive Gaussian noise is a well-studied problem and, when the interfering users are considered purely as additive noise, the interference-plus-noise process remains Gaussian with straightforward definitions in terms of the mean and variance (power) of the component noise and interference processes.

A TH-UWB signal, by contrast, has a low duty cycle; i.e., the frame duration is much longer than the pulse duration, and only a single pulse is transmitted per frame. A given chip slot sees interference from relatively few users compared to the number of interfering user links that may be simultaneously communicating. Also, both the propagation characteristics of UWB signals, and the motivating applications for UWB systems, suggest a small number of interfering users at close range. This is in contrast to some CDMA systems which have a wide coverage area and many contributing interferers of lower relative power. For example, several UWB devices may be situated within a small area in a residential living room and contribute most of the interference power, while the greater number of UWB devices situated in other parts of the residence or the neighborhood have much greater path loss and thus much smaller interfering impact on the desired link.

These properties, intuitively, lead to an interference pdf that is not Gaussian. Moreover, an interfering TH-UWB signal is impulse-like by definition ("impulse radio"), with the impulses having random arrivals due to the pseudo-random hopping code and random user delays. The interference process therefore intuitively resembles impulsive noise, not Gaussian noise.

The MUI in systems using both oversimplified (for the purposes of exposition) pulse models as well as practical UWB pulses has been investigated in [17] and the pdf of the

[2] In addition to a small number of interferers, the relative high powers of the interferers also hinders convergence to a Gaussian distribution.

MUI is discussed in detail in [17] and [18], [19]. Several key observations are made that explain the slow convergence of the UWB MUI to a Gaussian distribution via the Central Limit Theorem. First, the pdf has an impulse at the origin (zero amplitude) with magnitude equal to $(1-2D)^{N_u-1}$ where D is the duty cycle of the UWB waveform, roughly equal to the pulse duration divided by the frame duration, and N_u is the number of users in the system. It is noted in [18], [19] that the duty cycle is necessarily low since it is desireable to design the system so the frame duration T_f is greater than the delay spread of the channel, and the propagation characteristics of the channel dictate that the delay spread of the channel is much greater than the pulse duration. The duty cycle is also small due to the time-hopping design, where only one pulse is transmitted per frame; a low duty cycle gives the pulse room to hop in the frame.

It is futher observed in [17] and [18], [19] that the MUI pdf has other singularities due to zeros in the derivative of the pulse autocorrelation function. This can be inferred from the work of [20]–[23], where the MUI has been written as a function of the pulse autocorrelation with a random variable in the argument of the pulse autocorrelation. Using standard techniques [24], the pdf of the MUI can be written as a function of the pdf of this random variable, a function which includes the derivative of the pulse autocorrelation in its denominator. Thus, zeros in the derivative become singularities in the MUI pdf. Such singularities are not easily accommodated in closed-form expressions for the pdf, nor would the resulting pdf be useful for optimal receiver design. The pdf of a sum of independent random variables is given by the convolution of the component pdfs; the pdf of the interference sum over users and frames inherits some singularities from the component pdfs. Therefore, the convergence to a Gaussian pdf is slow with respect to the number of terms in the sum. For UWB systems, where the number of significant interferers may be few, a Gaussian approximation can fail.

Multipath is particularly material in UWB systems, where short-range indoor environments have a rich set of reflection and refraction surfaces to form paths. Moreover, the multipath delay profile is typically of much greater duration than the transmitted pulse, and assumptions made on the basis of ultra-short UWB pulses must be evaluated in the light of a much longer channel response. A multipath channel might be expected to improve the convergence to a Gaussian pdf somewhat, in that it effectively lowers the duty cycle of the received signal for a particular interferer so a given chip slot sees a greater number of independent interfering signals. However, an assumption of convergence of the interference pdf to a Gaussian distribution at a particular finger of a Rake receiver (to be discussed in Section V) still may not be accurate, as will be seen in the sequel.

B. MUI Modeling

Since determining an exact expression for the pdf of the MUI in a TH-UWB system is not straightforward and because the exact distribution would not be compactly expressed, it is necessary to consider modeling MUI with probability distributions that are both sufficiently accurate, and tractable for receiver design and performance analysis. The Gaussian distribution, as discussed above, is tractable but not an accurate model. A number of other distributions have been considered. These distributions have in common that they model processes which are more impulsive than the Gaussian process, with pdfs that have heavier tails than the Gaussian process (i.e., a higher probability of larger-magnitude events). Three key criteria in developing a suitable model are the accuracy of the model, the extensibility of the MUI model to a model for MUI plus additive Gaussian noise, and the utility of the model for synthesis of practical receiver designs.

A number of authors have considered the distribution of MUI in UWB systems and performance of UWB systems in the presence of MUI, e.g. [18]–[23], [25]–[49]. Early results used a Gaussian approximation to the interference in determining bit-error rates (BERs) for TH-UWB systems [3], [4], [50]–[52]. However, Gaussian approximations were shown to significantly underestimate the BER [10], [20], [26], [27] of UWB systems for medium to large SNRs, i.e., the SNR region where MUI is the significant impairment, motivating non-Gaussian analysis and designs. A number of non-Gaussian distributions have been considered for IR-UWB MUI or MUI plus noise, such as the Laplace distribution [28]–[33], the Gaussian-Laplace mixture distribution [18], [19], the generalized Gaussian distribution [34], [37], [38], the Gaussian mixture distribution [32], [33], [44], [49], the Middleton Class-A noise distribution [25], [32], [33], and the symmetric alpha-stable distribution [31], [41], [42], [53], [54]. Table I lists properties for each of these distributions.

For a binary communication system with a noise-plus-interference pdf that is symmetric about the origin, the BER of a constant threshold detector with equal energy symbols is directly proportional to the area of a tail region of the pdf [18], [19], [55]. The results of [20]–[22] suggest that the Gaussian distribution has insufficient area in the tails to accurately model UWB MUI (Fig. 2). A measure of the heaviness of the tails of the MUI pdf is the excess kurtosis [18], [19], [34], [36]

$$\varrho_I = \frac{\boldsymbol{E}\{I^4\}}{[\boldsymbol{E}\{I^2\}]^2} - 3. \tag{5}$$

A positive kurtosis indicates a distribution with heavier tails than the Gaussian distribution, suggesting that the true UWB MUI, and more appropriate models, have positive excess kurtosis. This is supported by results in [18], [19], [34], where the excess kurtosis of the total interference I, and the interference in each frame, I_i, is determined by simulation. The results from [19] are duplicated in Table II, where ϱ_I denotes the kurtosis of the total MUI for one symbol, and ϱ_{I_i} denotes the kurtosis of the partial MUI components in one frame. The distribution of the correlator output for a particular frame is seen to deviate significantly from a Gaussian distribution ($\varrho = 0$) even for a relatively large number of interferers.

The Laplace distribution is a common model for impulsive noise [56], [57], and receivers designed to operate in a MUI environment modeled by a Laplace distribution have been presented in [28]–[30]. To support this, the empirical pdf of the interference and the Laplace pdf have been plotted in [30]

TABLE I
PROBABILITY DISTRIBUTIONS CONSIDERED FOR MODELING MUI.

Name	pdf	Parameters	Comments
Gaussian	$f_R(r) = \frac{1}{\sqrt{2\pi}\sigma} \exp\left(-\frac{(r-\eta)^2}{2\sigma^2}\right)$	η =mean σ^2 = variance	poor model for MUI
Laplace	$f_R(r) = \frac{1}{2c} \exp\left(-\frac{\lvert r-\eta\rvert}{c}\right)$	η = mean $2c^2$ = variance	good approximation to MUI alone
Gaussian-Laplace mixture	$f_R(r) = \frac{\exp(\sigma^2/2c^2)}{2c}[\exp\left(\frac{r}{c}\right) Q\left(\frac{r}{\sigma}+\frac{\sigma}{c}\right)$ $+\exp\left(-\frac{r}{c}\right) Q\left(-\frac{r}{\sigma}+\frac{\sigma}{c}\right)]$	σ from Gaussian c from Laplace	intuitive: Laplace-modeled interference plus AWGN
Generalized Gaussian	$f_R(r) = \frac{1}{2\Gamma(1+1/p)A(p,\sigma)} \exp(-\left\lvert\frac{r-\eta}{A(p,\sigma)}\right\rvert^p)$	p = order (shape) η =mean σ^2 = variance $A(p,\sigma)$ def. in §IV-H	Laplace and Gaussian are special cases; can adapt between the two
Cauchy	$f_R(r) = \frac{\zeta}{\pi[(r-\mu)^2+\zeta^2]}$	μ =location ζ = scale	α-stable with $\alpha = 1$; pdf and opt. detector known. Models MUI only. Infinite second moment.
Symmetric α-stable	unknown for general α CF $\Phi(\omega) = \exp(-\zeta\lvert\omega\rvert^\alpha + j\omega\mu)$	α = char. exponent (shape) μ =location, ζ = dispersion	Cauchy and Gaussian are special cases, but general pdf unknown and opt. detector impractical. Infinite second moment.
Gaussian mixture	$f_R(r) = \sum_{l=1}^{L} \frac{\lambda_l}{\sqrt{2\pi\sigma_l^2}} \exp\left(-\frac{r^2}{2\sigma_l^2}\right)$	L $\{\lambda_1,\ldots,\lambda_L\}$ $\{\sigma_1^2 \ldots \sigma_L^2\}$	excellent fit to simulation but many parameters to estimate; accommodates AWGN
Middleton Class-A	$f_R(r) = \sum_{i=0}^{N} \frac{A^i e^{-A}}{i!\sqrt{2\pi\sigma_i^2}} \exp\left(-\frac{r^2}{2\sigma_i^2}\right)$	A, N, $\{\sigma_1^2,\ldots,\sigma_N^2\}$	good fit to simulation; expressible in terms of system parameters; accommodates AWGN

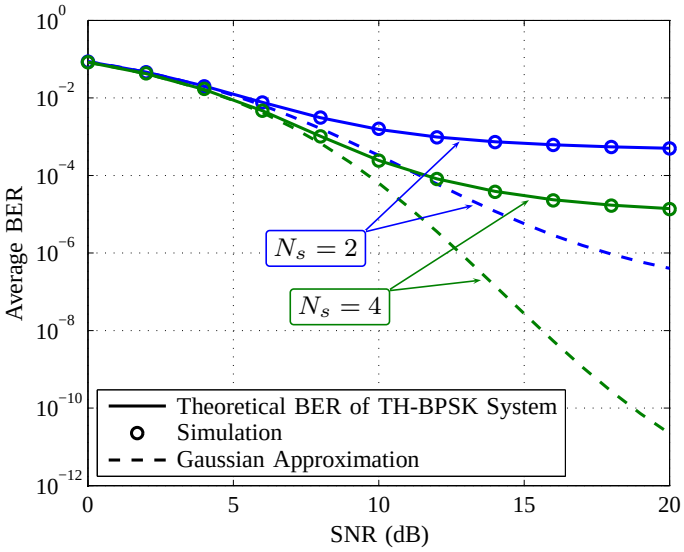

Fig. 2. The average BER of a TH-BPSK system versus SNR for a repetition code with $N_s = 2$ and $N_s = 4$ assuming seven asynchronous interferers (from [22]).

TABLE II
FROM [19], EXCESS KURTOSIS OF A SIMULATED MUI PROCESS.

N_u	N_h	N_s	T_f	ϱ_I	ϱ_{I_i}
128	32	8	28.8	0.1695	0.7813
128	16	8	14.4	0.1038	0.3885
25	16	4	20	1.1765	2.8914
25	8	8	20	1.0027	2.4084
16	8	8	20	1.5425	3.5577
16	8	4	20	2.0501	4.5758

and shown to have close resemblance, particularly in the tail region where the Gaussian pdf deviates significantly from the empirical pdf of the MUI (Fig. 3). MUI simulations also are provided for three and 15 interferers in [19], reproduced here in Fig. 4. Fig. 4(a) shows the Laplace distribution to be a better match to the simulated interference for three interferers and Fig. 4(b) shows the Laplace distribution to be a good match to the simulated interference for 15 interferers. The Laplace distribution has an excess kurtosis of 3, and based on Table II should be superior to a Gaussian approximation to model both the total interference and the frame interference. The Laplace distribution also has been found in [58], [59] to more closely approximate the sum of inter-chip, inter-path, and inter-symbol interference in UWB Rake reception than a Gaussian approximation.

A model based on the addition of a Laplace process, representing the MUI, to an AWGN process, representing the ambient noise, is examined in [18], [19], and optimal and suboptimal receivers are designed based on this Gaussian-Laplacian model.

The generalized Gaussian pdf is considered as a model for the total disturbance (MUI plus noise) in [34]–[38]. The generalized Gaussian pdf has a parameter, denoted p in [37], [38], which changes the shape of the distribution and allows for adaptation to various channel conditions. The results show

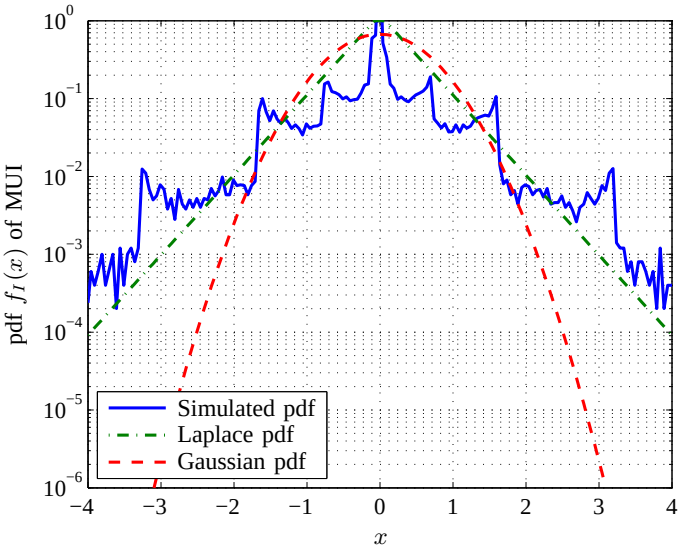

Fig. 3. Comparison of the pdf of the total MUI for fifteen interfering UWB signals obtained from simulation, the Laplace approximation, and the Gaussian approximation (from [30]).

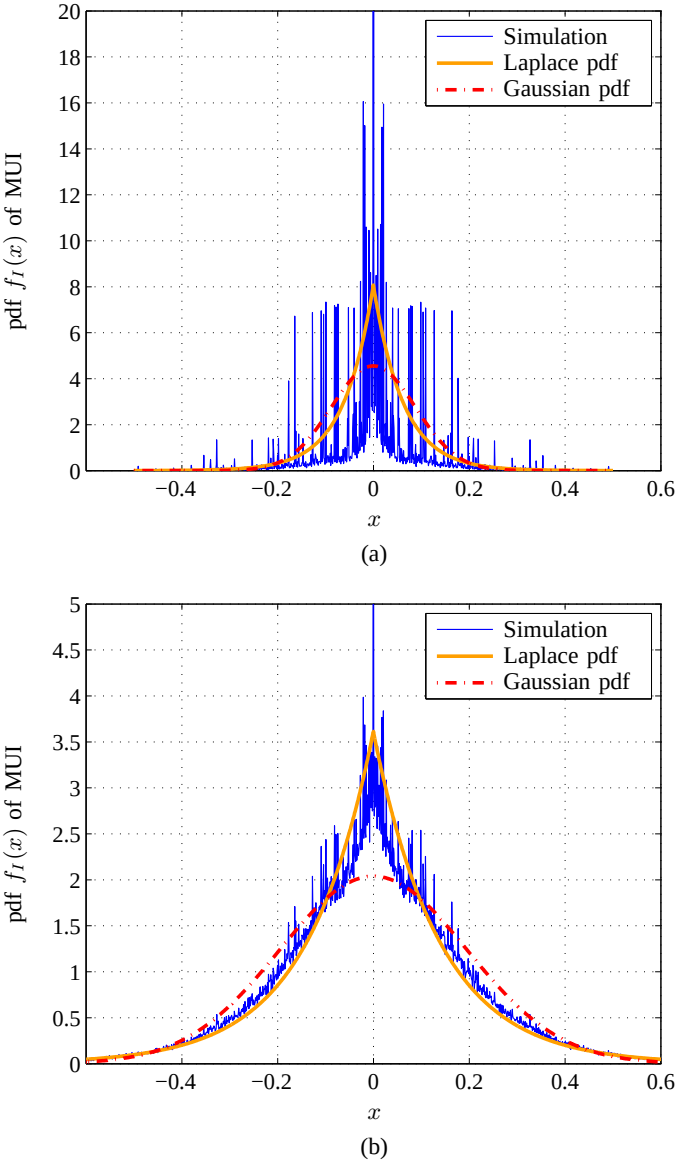

Fig. 4. A comparison of the pdf of the MUI with Gaussian and Laplacian approximations for (a) three interferers, (b) fifteen interferers (from [19]).

the generalized Gaussian pdf to be a flexible class of pdfs to model the disturbance. When Gaussian noise is dominant, the generalized Gaussian pdf yields exactly the Gaussian pdf with $p = 2$. As MUI becomes more significant, lower values of p make the pdf better fit the observed disturbance. The Laplace distribution, useful for modeling MUI alone and discussed above, is a special case for $p = 1$. Values of p less than unity give more impulsive distributions than the Laplace distribution. Thus, the generalized Gaussian distribution offers much flexibility in MUI-plus-noise modeling. Plots of the empirical pdf of the noise-plus-interference for a TH-UWB system are provided in [37] for SIR $= 10$ dB and different SNR values (Fig. 5). It is observed in [37] that for low SNR the pdf of Y_i is approximately Gaussian and $p \approx 2$ is appropriate. For moderate SNR the pdf can be approximated as the Laplace distribution with $p = 1$, while for high SNR a value of $p < 1$ is appropriate. The generalized Gaussian pdf also lends itself to obtaining tractable, practical receiver designs analytically.

The symmetric alpha-stable class of probability distributions [60]–[62] has received recent interest for modeling UWB MUI. The Gaussian distribution is the stable distribution with $\alpha = 2$ and the Cauchy distribution is stable with $\alpha = 1$. Stable distributions with $\alpha < 2$ are suitable for modeling data with large fluctuations and have been used to model impulsive noise. The parameter $\alpha \in (0, 2]$ determines the shape of the pdf, with lower α yielding more impulsive distributions with heavier tails. Except for $\alpha = 2$, stable distributions have algebraic tails and infinite variance. The use of a symmetric alpha-stable distribution to model the interference in TH-UWB has been examined in [31] by considering a smoothed pdf of simulated MUI. Other distributions compared were the Gaussian distribution, generalized Gaussian distribution, Laplace distribution, and Cauchy distribution. The smoothing, which removes the singularities in the empirical pdf, is justified in [31] and results in a meaningful graphic comparison, duplicated here in Fig. 6. It is seen that the alpha-stable distribution provides an excellent match to the tail behavior of the MUI when α is estimated using the method of [31] (see Section VI). Since the tail behavior is critical in determining the BER, this suggests a symmetric alpha-stable distribution is an excellent candidate for modeling UWB MUI.

References [32], [33] compare the suitability of the Gaussian approximation, the Gaussian mixture (GM) distribution, the Middleton Class-A (MCA) noise distribution, and the Laplace distribution for modeling MUI in TH-UWB systems. A GM distribution, which has a pdf given by a weighted mixture of Gaussian pdfs with different variances, has been used in [44] to model MUI in an infrared UWB application, using the expectation-maximization (EM) algorithm [63] to determine the parameters of the model. It has been proposed in [25] to model MUI by a MCA noise distribution [64], which also has been widely used for modeling impulsive noise. The pdfs of the total MUI under each assumption,

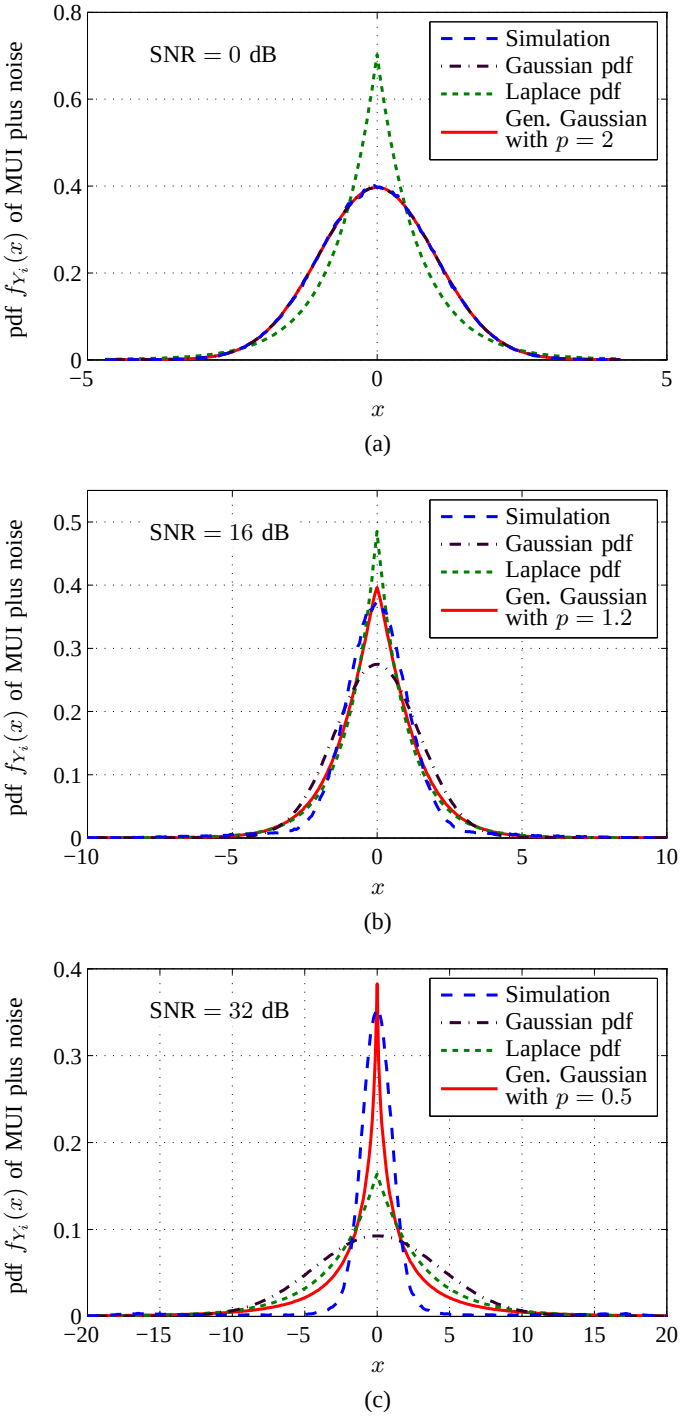

Fig. 5. The simulated pdf of the amplitude of the total disturbance sample (noise plus interference) in each frame, plotted with the Gaussian pdf, the Laplacian pdf, and the generalized Gaussian pdf for different values of p. (a) SNR = 0 dB, (b) SNR = 16 dB, (c) SNR = 32 dB (from [37]).

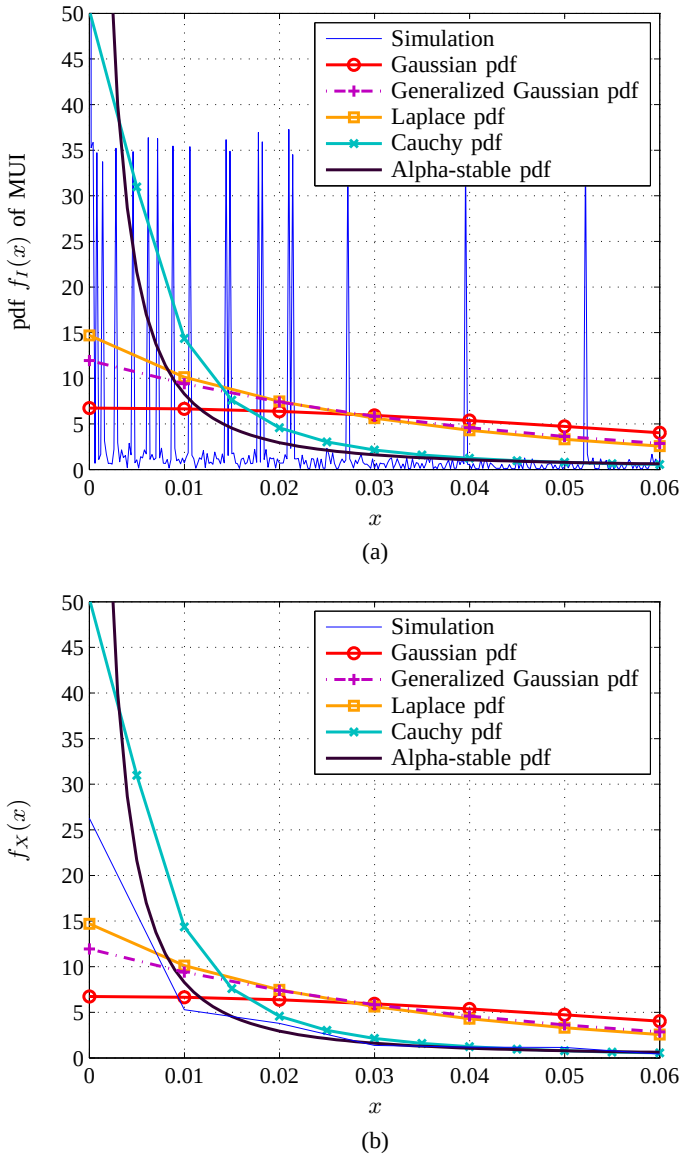

Fig. 6. Approximations to the simulated MUI pdf, (a) before smoothing, (b) after smoothing (from [31]).

and the pdfs of the MUI plus noise, were compared in [32], [33] by simulation. In addition, the predicted BER under each approximation was compared to the exact BER analysis reported in [21]. It was noted that the Gaussian approximation did not represent the impulsive component and heavier tails of the simulated pdf, and that the significantly lighter tail region would predict the significantly underestimated BER results revealed in [21]. Based on the pdf comparison, the GM and MCA distributions are reported in [32], [33] to be the better approximations of those considered, with the GM model most closely matching the tail region (Fig. 7). The presented BER results (Fig. 8) confirm that the GM model provides good BER estimates. However, it was found that the number of iterations used in the EM algorithm was critical for providing accurate BER estimates, and in particular the small number of iterations reported in [44] to estimate the pdf was insufficient to accurately estimate the BER. It is also noted in [32], [33] that while the MCA model and GM model both can be written as a sum of Gaussian pdfs, the parameters for the MCA model can be determined from the UWB system parameters with much less computational complexity than determination of the GM model parameters by the iterative EM algorithm, based on noisy channel samples for each SIR value and SNR value. The Laplace-based model was, in both the pdf plots and in the BER results, seen to be farther from the exact case than the

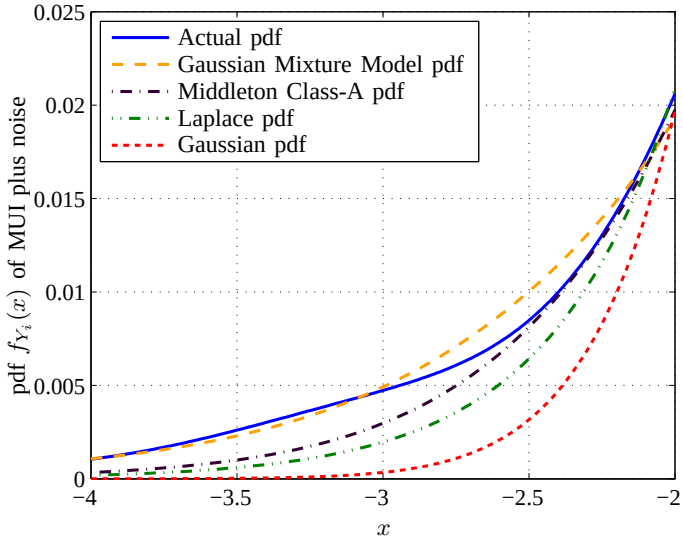

Fig. 7. A comparison of the pdf tails of the GMM, MCA, Laplace, and Gaussian approximations with simulation (from [32]).

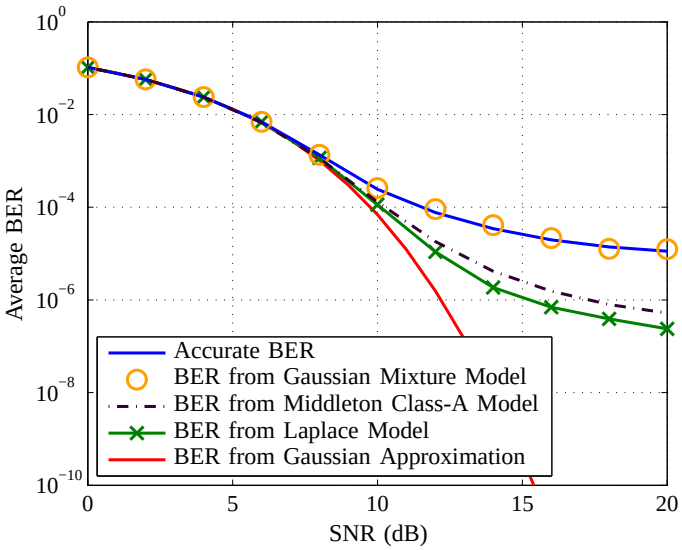

Fig. 8. The average BER of a TH-PPM UWB system versus SNR with $N_s = 4$, estimated using the different methods (from [32]).

GM or MCA models, underestimating the BER. However, it can be seen in Fig. 8 that the difference between the predicted BERs for the MCA and Laplace-based models and the true BER is much smaller than the difference between the BER predicted by the Gaussian approximation and the true BER. All of the impulsive-based models capture the error-rate floor behavior observable in the accurate BER, while the Gaussian model completely fails to capture the moderate to high SNR performance of the system. It is clear, irrespective of the exact form of distribution, that distributions suitable for impulsive noise are a much better fit to the MUI statistics than a Gaussian pdf. Summary comments on each model can be found in Table I.

IV. Design of TH-UWB Receivers for Superior Performance in MUI

In Section III we have provided considerable evidence that the MUI in UWB systems is not well modeled by a Gaussian distribution. In view of these conclusions, there is potential benefit to be gained in bit error rates (or outage rates, or other system performance indicators) by designing receivers that are appropriate for signals embedded in an accurately-modeled MUI background, and that are able to adapt to channels where MUI is a dominant impairment. Moreover, a demonstrated performance enhancement obtained with such novel receivers will further justify the underlying models. In this section, we start with a general example of detection in non-Gaussian noise, and then describe several recently proposed receivers that offer superior performance in MUI in comparison to the conventional UWB receiver.

Realistic UWB system analysis must include the effects of a multipath channel, and practical UWB system designs must be able to cope effectively with multipath. Nonetheless, analysis, modeling, and design of UWB systems operating in single-path channels is useful. First, novel designs can be motivated and described most clearly in a single-path channel. Second, often the key design principles developed for the single-path case can be readily extended to novel designs for the multipath channel. In this section we first describe and evaluate all proposed receivers in the single-path (AWGN) channel, then the corresponding receivers adapted for a multipath channel will be presented in Section V.

A. Optimal Detection in Non-Gaussian Noise

As a starting point, suppose that in a generic communications system we have N samples $\{r_i\}_{i=0}^{N-1}$ of a signal received in additive noise, with $r_i = Ad + n_i$. The binary symbol d takes a value in $\{-1, 1\}$, A is a nonnegative scalar amplitude, and $\{n_i\}$ are additive noise samples. Let the samples r_i be independent with a common pdf $f_R(r)$. The maximum-likelihood (ML)-optimum receiver minimizing the overall probability of error bases its decisions on the log-likelihood ratio [56], [57]

$$\Lambda = \sum_{i=0}^{N-1} \log \frac{f_R(r_i|d=+1)}{f_R(r_i|d=-1)}. \tag{6}$$

That is, the decision statistic is the sum of the log-likelihood ratios for each sample considered individually. Considering the case of equiprobable source symbols for simplicity, the decision on the transmitted bit is made according to

$$\begin{aligned} \Lambda > 0 &\Longrightarrow d = 1 \\ \Lambda < 0 &\Longrightarrow d = -1. \end{aligned} \tag{7}$$

The case $\Lambda = 0$ can be decided by a fair coin toss. This decision rule is valid for any pdf $f_R(r)$, i.e. any noise distribution.

In the particular case where the noise has a Gaussian distribution with zero mean and variance σ^2, the received signal has pdf

$$f_R(r_i) = \frac{1}{\sqrt{2\pi}\sigma} \exp\left(-\frac{(r_i - dA)^2}{2\sigma^2}\right) \tag{8}$$

and the log-likelihood ratio after simplification becomes

$$\Lambda = \frac{2A}{\sigma^2} \sum_{i=0}^{N-1} r_i. \tag{9}$$

That is, in the Gaussian case the optimal detector takes the sum of the samples of the received signal and compares this sum with the threshold zero. (The multiplicative constant is irrelevant to the decision.) The summand r_i is a *partial decision statistic* for the ith sample.

We emphasize that while (6) and (7) are valid for any noise pdf, (9) is optimal only for the Gaussian pdf. Thus, when the background noise plus interference is not Gaussian-distributed the receiver based on (9) is not an optimal receiver.

A non-Gaussian example from [57], which will be important in the sequel, is the case in which the noise samples $\{n_i\}$ have a Laplace distribution and therefore the received signal has pdf

$$f_R(r_i) = \frac{1}{2c} \exp\left(-\frac{|r_i - dA|}{c}\right) \tag{10}$$

where $c > 0$ is a scale parameter. In this case the log-likelihood ratio (6) is

$$\Lambda = \frac{2}{c} \sum_{i=0}^{N-1} \left(\left| \frac{r_i}{2} + \frac{A}{2} \right| - \left| \frac{r_i}{2} - \frac{A}{2} \right| \right). \tag{11a}$$

Again, the form is a sum over partial decision statistics $(|r_i + A| - |r_i - A|)/2$ for each sample. However, the partial decision statistic now is formed as a *nonlinear* operation on r_i, which can be written as

$$\left| \frac{r_i}{2} + \frac{A}{2} \right| - \left| \frac{r_i}{2} - \frac{A}{2} \right| = \begin{cases} A & r_i \geq A \\ r_i & -A < r_i < A \\ -A & r_i \leq -A. \end{cases} \tag{11b}$$

Thus, (11) applies a soft-limiting operation to the partial decision statistics before summation.

Note that the assumed independence between the samples r_i has been used in writing (9) and (11). This independence condition will not be met precisely in a UWB system [23]. A receiver which takes into account dependence between frames will, in theory, provide better performance. However, the independence assumption vastly simplifies both the analysis and receiver design; the goal of simple and practical receiver designs motivates ignoring the small dependence between frames at the design phase.

B. The Conventional UWB Receiver

Consider detection of the 0th bit of user 1, where the users transmit signals according to (2). The conventional single-user correlation receiver uses a correlation template waveform matched to the desired user's signaling waveform to form

$$r = \sum_{i=0}^{N_s-1} \int_{iT_f}^{(i+1)T_f} r(t) p\left(t - iT_f - c_i^{(1)} T_c\right) dt. \tag{12}$$

(Techniques for synchronization of UWB signals can be found, for example, in [65]-[68].) Since $r(t)$ is the sum of the desired signal, MUI, and noise, all of which are independent, we can define the partial decision statistic and write it as the sum of signal, MUI, and noise,

$$r_i = \int_{iT_f}^{(i+1)T_f} r(t) p\left(t - iT_f - c_i^{(1)} T_c\right) dt = S_f + I_i + N_i. \tag{13}$$

Note that the signal part of r_i is the same for all i, and can be written $S_f = A_c d_0^{(1)}$, where $A_c > 0$ is a scalar amplitude and $d_0^{(1)}$ is the zeroth bit of the first user, i.e. the symbol to be recovered by the detector. The amplitude A_c can also be thought of as the unsigned signal component in a single frame,

$$A_c = |S_f| = A_1 \sqrt{\frac{E_b}{N_s}} \tag{14}$$

where A_1 is the channel gain of the desired user.

The conventional matched-filter (CMF) linear receiver forms the decision statistic

$$\Lambda_{\text{CMF}} = \sum_{i=0}^{N_s-1} r_i \tag{15}$$

with the decision rule

$$\begin{aligned} \Lambda_{\text{CMF}} > 0 &\Longrightarrow d_0^{(1)} = 1 \\ \Lambda_{\text{CMF}} \leq 0 &\Longrightarrow d_0^{(1)} = -1. \end{aligned} \tag{16}$$

The conventional receiver is the BER-optimal coherent receiver for a signal in a background of Gaussian noise plus Gaussian interference and has been widely applied to UWB systems. The terms "conventional receiver," "linear receiver," and CMF have been used to describe this receiver. If the receiver filter or correlator is viewed as being matched to the entire symbol, then only the conventional receiver is such a matched filter and the CMF terminology is unambiguous.

One might not expect that one can improve upon the CMF UWB receiver performance, especially in a static channel. In particular, any binary signaling scheme can be converted to an equivalent binary antipodal signaling scheme [69] and, therefore, the detection of the signal ultimately reduces to a threshold comparison. The reason that a better UWB receiver design is possible is because of the frame structure of the UWB signal, i.e., the repetition code. The repetition code structure represents an inherent diversity system within the CMF UWB receiver. It is important to note that adding together the outputs from the correlators of the different frames is a ML structure in AWGN, but is not an ML structure in the presence of MUI which is not Gaussian. Simply adding the outputs of the correlators from all the frames is not an optimal processing of the frame correlator output signals.

C. Overview of Novel Receivers

Unfortunately, two problems arise in optimal receiver design. First, the exact pdf of the MUI in a UWB system cannot be compactly written (see Section III) and does not lead to tractable receiver designs. Second, the inevitable presence of Gaussian noise in the system means that the total noise-plus-interference has a complicated pdf that is the convolution of the exact MUI pdf with a Gaussian pdf, even less suggestive of

useful receiver designs. Moreover, the shape of the resulting pdf depends on the UWB system parameters and the time-varying noise and interference environment and may not be available *a priori*.

The challenge, therefore, is to obtain practical receivers that offer superior performance in MUI with no loss of optimality in AWGN, in the absence of the exact MUI-plus-noise pdf. This challenge has been approached in several different ways outlined in the sequel.

Section IV-D describes the soft-limiting UWB receiver, designed to detect a UWB signal in MUI having an approximating Laplace distribution. It will be shown that the soft-limiting receiver provides superior performance in MUI, but is not optimal in Gaussian noise. The remaining receivers to be discussed include the CMF receiver as a special case of the receiver parameters, and thus, theoretically with parameter adaptation optimal for the interference and noise conditions, can offer superior performance in MUI *and* no loss of performance in AWGN. That is, the receivers of Sections IV-E through IV-J can always provide performance that meets or exceeds both the CMF receiver and the soft-limiting UWB receiver. Practical or model-based parameter estimation can impact the optimality of specific receiver designs, however, in some channel conditions.

The adaptive soft-limiting receiver of Section IV-E extends the soft-limiting receiver, matching the soft-limiting threshold to the SNR and SIR of the channel. The Gaussian-Laplacian mixture receiver of Section IV-F and the simplified Gaussian-Laplacian mixture receiver of Section IV-G are designed to detect a signal in a background of interference plus AWGN, where the interference has an approximating Laplace distribution. The p-order metric receiver, p-order adaptive-threshold-limiting receiver and myriad filter receiver of Sections IV-H and IV-I each consider approximating distributions to the MUI-plus-noise that contain the Gaussian distribution as a special case, allowing adaptation between MUI and Gaussian environments with no loss of optimality in the Gaussian case. Lastly, the zonal receiver to be described in Section IV-J is based on observations made for simulated MUI pdfs, and again can be adapted to provide no loss of optimality in a pure AWGN environment.

Zero-threshold detection is unaffected by multiplication of the detection statistic by a positive constant. In order to unify the treatment of the various receivers, some of the nonlinearity functions presented in this paper have been scaled from those found in the original references. A unified block diagram of all the proposed receivers is given in Fig. 9.

None of the receivers considered here are optimal for TH-UWB, except in the limiting case where MUI is absent and the only impairment is AWGN. The design of an optimal receiver would require a tractable expression for the pdf of the interference plus noise in a TH-UWB system. However, with reasonable additional complexity over the CMF receiver, each receiver described here shows superior performance in MUI and, with the exception of the non-adaptive receiver of Section IV-D, no loss of performance in AWGN when optimized to the TH-UWB noise-plus-interference conditions. Table III summarizes the advantages and disadvantages of each

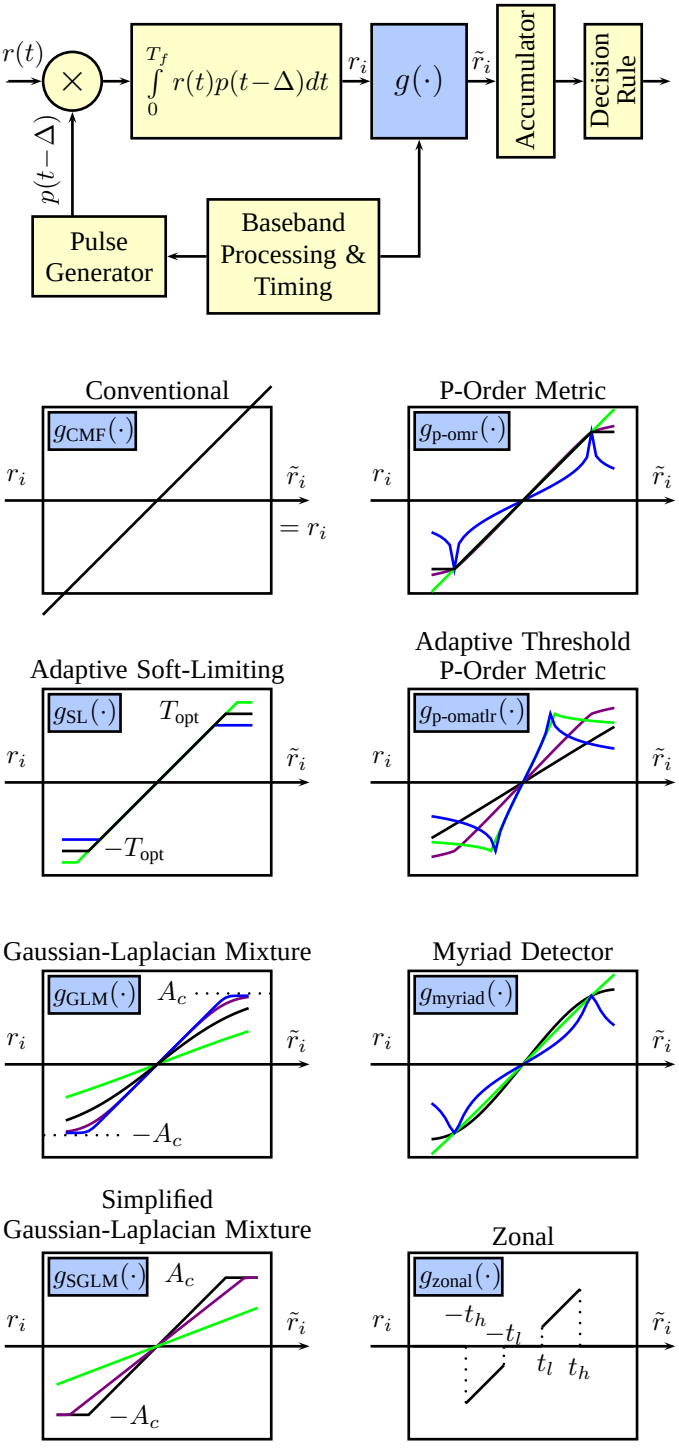

Fig. 9. Unified block diagram of the novel receiver structures.

TABLE III
A SUMMARY OF SOME ADVANTAGES AND DISADVANTAGES OF EACH RECEIVER.

Receiver	Advantages	Disadvantages
CMF	optimal in absence of interference; less complex	inferior performance in low SIR; does not adapt to noise and interference conditions
Soft-Limiting	simple nonlinearity; good performance for low SIR/high SNR; no channel information required beyond A_1	inferior to CMF for low SNR/high SIR; does not adapt to noise and interference conditions
Adaptive-Threshold Soft-Limiting	simple nonlinearity; performance always better than or equal to CMF	adapted thresholds are pre-simulated and stored in lookup table
GLM	nonlinearity function expressed in terms of functions of SIR and SNR; intuitive mixture; able to adapt over SNR/SIR	complicated nonlinearity function
SGLM	simple soft-limiting nonlinearity, but adaptive to channel conditions and better performance than soft-limiting receiver; nonlinearity expressed in terms of SIR and SNR	performance inferior to GLM for some noise and interference conditions
p-omr	very good performance; nonlinearity function can be expressed in terms of interference moments and SNR	nonlinearity function more complex than soft-limiter
p-omatlr	performance always better than or equal to both CMF and p-omr with same complexity of nonlinearity	adaptation based on pre-simulated values
Myriad Filter	excellent performance; nonlinearity expressed in terms of channel estimates	more complex nonlinearity; parameters require estimation of empirical characteristic function
Zonal	simple nonlinearity; very good performance	adapted thresholds use pre-simulated values stored in lookup table

receiver.

In order to streamline the presentation of the various receivers, discussion of algorithms for estimation of receiver parameters from channel data is deferred to Section VI.

D. The Soft-Limiting UWB Receiver

The first class of receiver designs to be considered are the soft-limiting designs of [28], [29], [30]. Motivated by the observation that the MUI in UWB is impulsive in nature, MUI is modeled in these receivers by the Laplace distribution, which is a traditional model for impulsive noise as discussed in Section III. The BER-optimal receiver for a constant signal in Laplace noise was given by example in (11), and is a standard result [56], [57], which was proposed as a basis for novel UWB receiver designs in [29].

The decision statistic for the conventional UWB receiver has been given in (15), a sum of the correlator outputs r_i for each frame. The soft-limiting detector proposed in [29], [30] forms a decision based on a sum of *transformed* correlator outputs $g_{\text{SL}}(r_i)$,

$$\Lambda_{\text{SL}} = \sum_{i=0}^{N_s-1} g_{\text{SL}}(r_i), \tag{17a}$$

where

$$g_{\text{SL}}(x) = \begin{cases} A_c, & A_c \leq x \\ x, & -A_c < x < A_c \\ -A_c, & x \leq -A_c. \end{cases} \tag{17b}$$

The transmitted information bit $d_0^{(1)}$ is decided according to the rule

$$\begin{aligned} \Lambda_{\text{SL}} > 0 &\Longrightarrow d_0^{(1)} = 1 \\ \Lambda_{\text{SL}} \leq 0 &\Longrightarrow d_0^{(1)} = -1. \end{aligned} \tag{17c}$$

The threshold A_c is the square root of the received signal energy in each frame for the desired user, as defined in (14).

Use of A_c as the threshold corresponds to the limiting threshold in (11). It is a sensible design choice since the signal component of r_i has an amplitude of A_c; when $|r_i| > A_c$ this is due to noise or interference.

The benefits of the soft-limiting structure in suppressing MUI are intuitive. The UWB pulse has a short duration relative to the frame duration. By design, time-hopping is used to ensure that collisions between the desired user and a given interfering user in successive frames are rare. Thus, many of the desired user's frames will see negligible interference from a given interfering user. When a collision occurs, the correlator output for the frame with a pulse collision may have a relatively large amplitude, having a large effect in the decision statistic sum Λ_{CMF} and yet a very small SIR making this effect deleterious. The soft-limiter moderates the effect of colliding pulses in the overall decision statistic.

Indeed, in simulations where the desired signal is corrupted by MUI only, the soft-limiting receiver shows better performance in terms of BER than the conventional receiver, with the performance benefit increasing at low SIR levels (Fig. 10(a)). The benefits of the soft-limiting receiver are especially significant for a small number of interfering users (Fig. 10(b)). As the number of interfering users increases, the

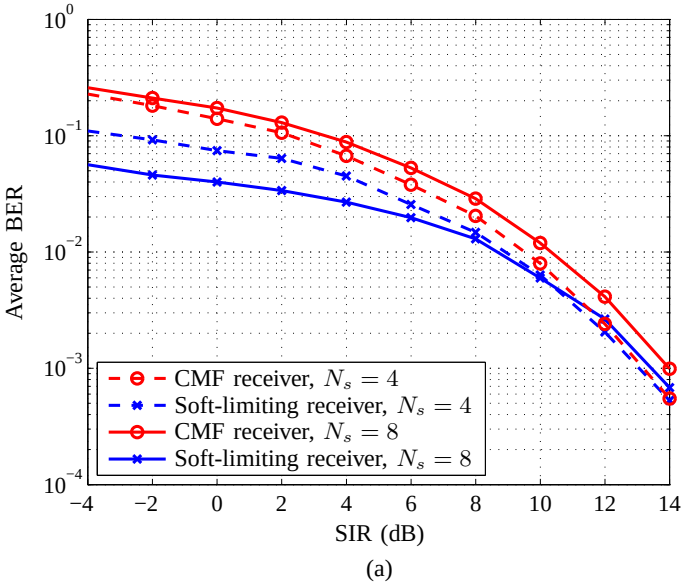

(a)

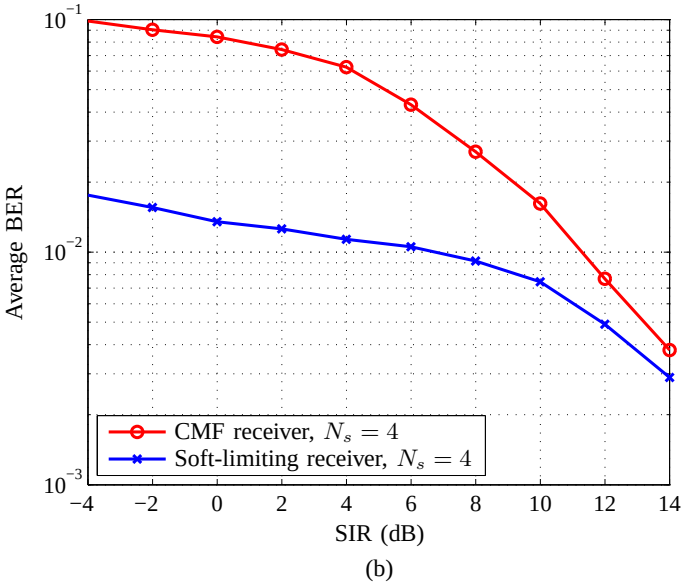

(b)

Fig. 10. The average BER versus SIR of soft-limiting and conventional TH-BPSK UWB receivers assuming (a) fifteen asynchronous interferers, (b) three asynchronous interferers (from [30]).

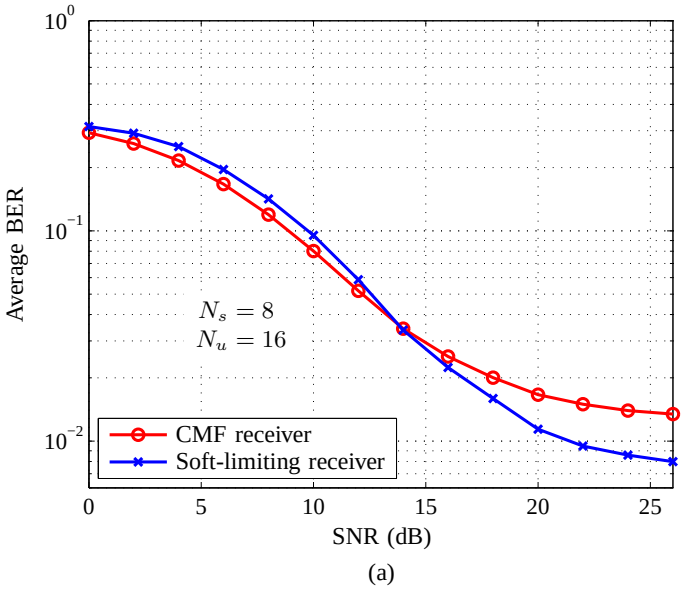

(a)

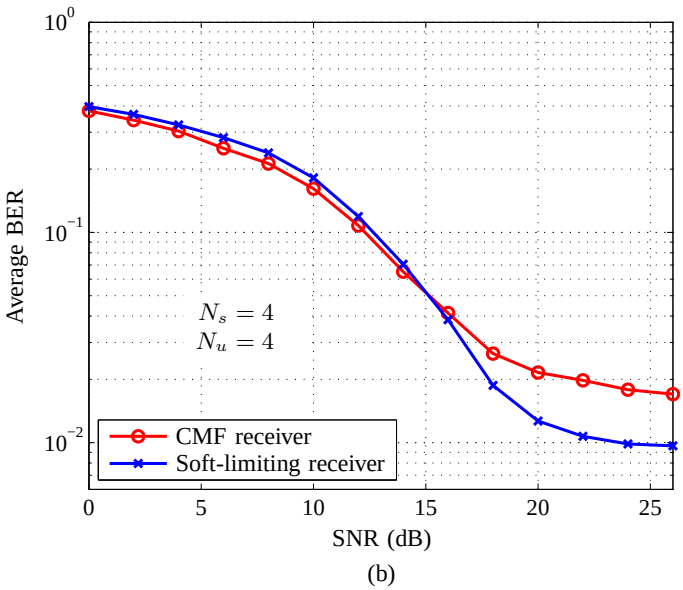

(b)

Fig. 11. The average BER versus SNR of soft-limiting and conventional TH-BPSK UWB receivers assuming (a) fifteen asynchronous interferers with $N_s = 8$, (b) three asynchronous interferers with $N_s = 4$ (from [30]).

interference pdf becomes closer to a Gaussian pdf, and the conventional receiver becomes closer to an optimal receiver. This is important since, as discussed in Section III, the short-range nature of UWB signals suggests a few dominant interferers located close to the receiver. However, the improvement of the soft-limiting receiver is seen throughout the SIR range and for both interference environments considered.

More relevant is the performance of the receiver when both MUI and AWGN are considered, since the soft-limiting receiver will be suboptimal in an AWGN-only environment. It can be seen in Fig. 11 that there is a crossover threshold in SNR, below which the BER for the conventional receiver is less than that of the soft-limiting receiver, and above which the soft-limiting receiver is superior. This motivates an adaptive version of the soft-limiting receiver that always obtains superior performance, discussed in the following section.

E. The Adaptive-Threshold Soft-Limiting Receiver

The conventional receiver is optimum when the only channel corruption is AWGN. The soft-limiting receiver is not optimal in this case and it is expected, and observed in Fig. 11, that the performance of the soft-limiting receiver is worse than the conventional receiver for high-SIR–low-SNR regimes, i.e., where Gaussian noise is the dominant impairment. However, it is noted in [30] that the soft-limiting receiver is identical to the conventional receiver when the limiting threshold is set to infinity. Therefore, an adaptive implementation is proposed in [28], [30] in which the threshold T_{opt} is optimized to minimize BER. The receiver computes

$$\Lambda_{\text{ASL}} = \sum_{i=0}^{N_s-1} g_{\text{ASL}}(r_i) \tag{18a}$$

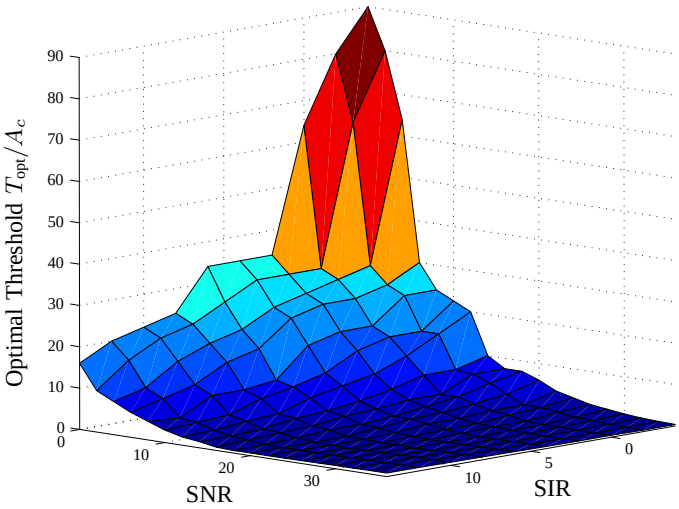

Fig. 12. The normalized optimal threshold values of the adaptive-threshold soft-limiting receiver for different values of SNR and SIR, assuming three asynchronous interferers (from [30]).

where

$$g_{\text{ASL}}(x) = \begin{cases} T_{\text{opt}}, & T_{\text{opt}} \le x \\ x, & -T_{\text{opt}} < x < T_{\text{opt}} \\ -T_{\text{opt}}, & x \le -T_{\text{opt}}. \end{cases} \tag{18b}$$

The parameter T_{opt} is the chip-correlator output amplitude threshold at which limiting takes place, with $T_{\text{opt}} \ge 0$. The transmitted information bit $d_0^{(1)}$ is decided according to the rule

$$\begin{aligned} \Lambda_{\text{ASL}} > 0 &\Longrightarrow d_0^{(1)} = 1 \\ \Lambda_{\text{ASL}} \le 0 &\Longrightarrow d_0^{(1)} = -1. \end{aligned} \tag{18c}$$

Since the parameter T_{opt} being optimized yields the conventional receiver as a special case, with a BER-optimized threshold the adaptive-threshold soft-limiting receiver can do no worse than the conventional receiver. Furthermore, the performance of the soft-limiting receiver as shown in Figs. 10-11 reveals that, for certain noise-plus-interference conditions, the adaptive soft-limiting receiver will perform much better than the conventional receiver. Thus, the soft-limiting receiver can always match or outperform the conventional receiver when the threshold is optimally chosen according to the noise and interference environment; the adaptation of the threshold yields the Gaussian-optimal and Laplacian-optimal receivers as special cases.

The BER-optimizing threshold T_{opt} is found by simulation in [30] and is a function of both SNR and SIR (Fig. 12). The implementation suggested in [30] is for the receiver to estimate these parameters (see Section VI), and then use a lookup table prewired into the receiver to determine the appropriate threshold T_{opt}.

F. The Optimal Gaussian-Laplacian Mixture Receiver

A different technique to design a receiver for detection in both Gaussian noise and non-Gaussian interference has been proposed in [18], [19]. The receiver of [18], [19] is optimized for a channel with a *mixture* of Laplacian and Gaussian noise; i.e., the impairment is the sum of a Laplace process and a Gaussian process, representing MUI and noise, respectively.

Consider again the partial correlation for the ith frame as defined in (13), $r_i = S_f + I_i + N_i$, and let the interference I_i have a Laplacian pdf (10) with parameter $c = \boldsymbol{E}\{I_i^2\}/2$, where $\boldsymbol{E}\{\cdot\}$ denotes the expected value. Let the noise N_i have a zero-mean Gaussian pdf (8) with $\sigma_n^2 = N_0/2$, and $S_f = A_c d_0^{(1)}$ as previously. Denote the sum of noise plus interference in the ith frame as $Y_i = I_i + N_i$. Since the noise and the interference are independent, the pdf of the sum Y_i can be obtained by a convolution of the pdf of I_i with the pdf of N_i. The result is given in [18], [19] as

$$\begin{aligned} f_{Y_i}(Y_i) = \frac{\exp(\sigma_n^2/2c^2)}{2c} \Bigg[&\exp\left(\frac{Y_i}{c}\right) Q\left(\frac{Y_i}{\sigma_n} + \frac{\sigma_n}{c}\right) \\ &+ \exp\left(-\frac{Y_i}{c}\right) Q\left(-\frac{Y_i}{\sigma_n} + \frac{\sigma_n}{c}\right)\Bigg] \end{aligned} \tag{19}$$

where $Q(\cdot)$ is the standard Gaussian Q-function $Q(x) = (2\pi)^{1/2} \int_x^\infty \exp(-t^2/2)dt$.

The ML-optimum receiver for a set of N_s independent observations of a signal embedded in noise-plus-interference having pdf (19) is determined in [18], [19]. The decision statistic is once again given by a nonlinear operation on the frame correlator outputs,

$$\Lambda_{\text{GLM}} = \sum_{i=0}^{N_s-1} g_{\text{GLM}}(r_i) \tag{20}$$

where

$$g_{\text{GLM}}(x) = \frac{c}{2} \ln \left[\frac{e^{\frac{x-A_c}{c}} Q\left(\frac{x-A_c+\sigma_n^2/c}{\sigma_n}\right) + e^{-\frac{x-A_c}{c}} Q\left(\frac{-x+A_c+\sigma_n^2/c}{\sigma_n}\right)}{e^{\frac{x+A_c}{c}} Q\left(\frac{x+A_c+\sigma_n^2/c}{\sigma_n}\right) + e^{-\frac{x+A_c}{c}} Q\left(\frac{-x-A_c+\sigma_n^2/c}{\sigma_n}\right)} \right]. \tag{21}$$

The transmitted bit is decided as $+1$ if $\Lambda_{\text{GLM}} > 0$ and -1 if $\Lambda_{\text{GLM}} \le 0$. (Note that (21) contains a normalization factor of $c/2$ not present in [18], [19].)

This receiver is optimal for independent observations in Laplacian interference plus Gaussian noise. It is not optimal for UWB because the interference process is only approximated by the Laplace distribution, and because the samples of the interference process are not strictly independent. However, the Gaussian-Laplace mixture (GLM) receiver demonstrates superior performance to the conventional receiver and superior performance to the fixed-threshold soft-limiting receiver of Section IV-D. Fig. 13(a) shows a comparison between the GLM detector, the soft-limiting detector of Section IV-D, and the conventional detector for a fifteen-interferer scenario and $N_s = 8$. The performance of the GLM detector is very close to that of the soft-limiting detector for high SNR, and very close to that of the conventional detector for low SNR. The performance of the GLM receiver always meets or surpasses those of the linear and soft-limiting detectors over the entire SNR range. However, for the three interferer case plotted in Fig. 13(b), it can be observed that for the smaller SNRs considered, the GLM receiver shows poorer

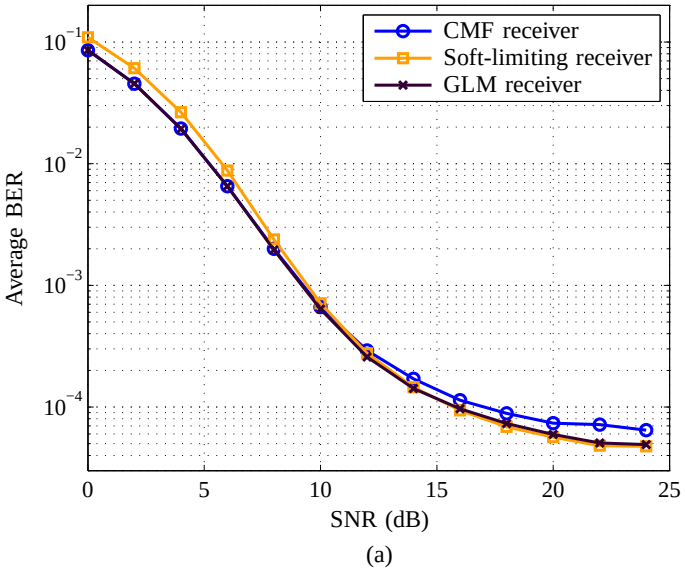

(a)

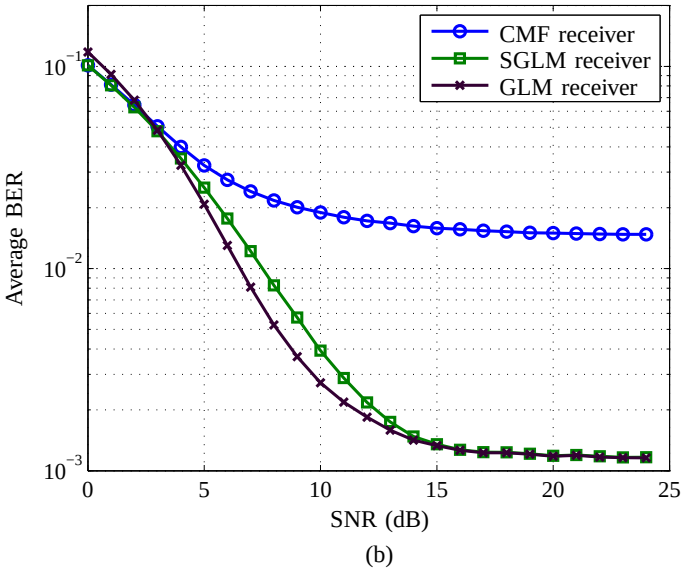

(b)

Fig. 13. (a) A comparison of the BERs of the GLM receiver, the soft-limiting receiver, and the linear CMF receiver for fifteen interferers (from [19]), (b) a comparison of the BERs of the GLM receiver and the SGLM receiver with the linear CMF receiver for three asynchronous interferers (from [70]).

performance than the linear CMF receiver. Fig. 4(a) reveals that the approximating Laplace distribution for the interference is a poorer fit for the three-interferer case than for the fifteen-interferer case. The GLM receiver, while optimal for the GLM model, is not optimal for TH-UWB MUI-plus-noise, and this becomes evident in some SNR and MUI conditions.

G. The Simplified Gaussian-Laplace Mixture Receiver

The GLM receiver is the optimal receiver for a signal received in a mixture of Laplacian interference and Gaussian noise, while the soft-limiting receiver of Section IV-D is the optimum receiver for Laplacian interference only and the conventional receiver is optimum for Gaussian noise only. The GLM is thus better matched to the mixture of MUI and AWGN in the channel. However, a comparison of the GLM

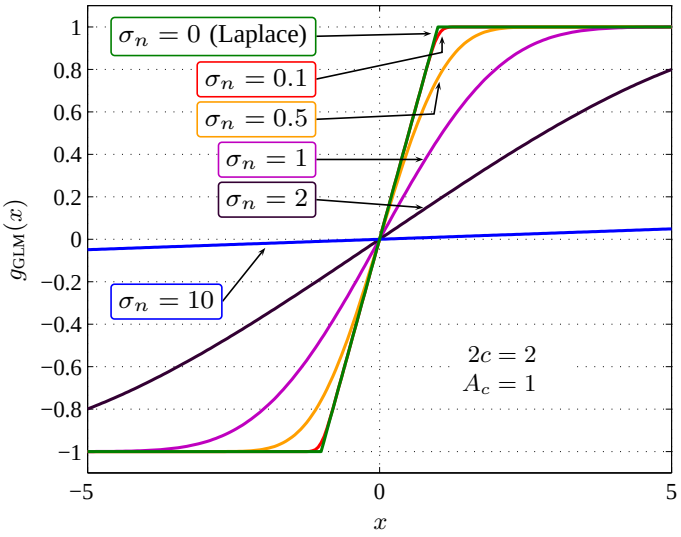

Fig. 14. The nonlinearity curves of the GLM detector for different values of σ_n, plotted with the soft-limiting detector characteristic (from [19], with altered normalization).

nonlinearity (21) with (11) or (9) shows the former to be much more complex. In [18], [19] an approximation to the optimum receiver is proposed which is simpler to implement yet achieves nearly the same performance.

The approximation starts with the observation (see Fig. 14) that in the limit as $x \to \infty$ the nonlinearity $g_{\mathrm{GLM}}(x) \to A_c$ while, in the limit as $x \to -\infty$, $g_{\mathrm{GLM}}(x) \to -A_c$. Moreover, for $\sigma_n \to 0$, the function g_{GLM} approaches g_{SL}, i.e. the Laplacian detector (or soft-limiter), while for σ_n large the nonlinearity curve becomes nearly a straight line, i.e., the conventional receiver. The simplified Gaussian-Laplace mixture (SGLM) receiver proposed in [18], [19] approximates the optimum nonlinearity $g_{\mathrm{GLM}}(x)$ with three line segments,

$$g_{\mathrm{SGLM}}(x) = \begin{cases} A_c, & mx > A_c \\ mx, & -A_c \le mx \le A_c \\ -A_c, & -mx < -A_c \end{cases} \tag{22}$$

where m is the slope of the optimum nonlinearity (21) at the origin, derived in [19] as

$$m = \frac{1 - \exp\left(\frac{2A_c}{c}\right) \frac{Q(A_c/\sigma_n + \sigma_n/c)}{Q(-A_c/\sigma_n + \sigma_n/c)}}{1 + \exp\left(\frac{2A_c}{c}\right) \frac{Q(A_c/\sigma_n + \sigma_n/c)}{Q(-A_c/\sigma_n + \sigma_n/c)}}. \tag{23}$$

The nonlinearity function g_{SGLM} can be equivalently written

$$g_{\mathrm{SGLM}}(x) = \left| \frac{mx}{2} + \frac{A_c}{2} \right| - \left| \frac{mx}{2} - \frac{A_c}{2} \right|. \tag{24}$$

(A normalizing constant $c/2$ not found in [18], [19] has been applied to (22)–(24).)

The nonlinearity function g_{SGLM} is similar to that of the soft-limiting receiver, except that the slope of the linear region in the soft-limiting receiver is always equal to unity while that of the SGLM receiver depends on the SIR and SNR. Thus, the SGLM receiver adapts to the noise and interference conditions by changing the slope of the linear region, while the adaptive soft-limiting receiver of Section IV-E adapts via changing the limiting thresholds. Both receivers contain the

conventional receiver and the Laplacian-optimal soft-limiting receiver as special cases. It is suggested in [19] that the slope function (23) can be precomputed as a function of SIR and SNR and used in the receiver implementation via a lookup table. The implementation of the SGLM receiver is thus much simpler than the GLM-optimal receiver.

Fig. 13(b) shows the performance of the SGLM detector plotted together with the performances of the GLM detector and the linear detector, for three interfering users. The optimal GLM detector has roughly 1 dB better performance at an SNR of 10 dB, but the performances of the SGLM and GLM detectors are close for high SNR. The SGLM performance is better than the GLM performance at low SNR in this example (recall that the GLM is optimal only when the interference is truly Laplace distributed). For the channel conditions of Fig. 13(a), with fifteen interfering users, the SGLM performance curve is visually nearly indistinguishable from that of the GLM detector (see [19]), suggesting that in practice the simpler implementation of the SGLM detector is worthwhile. For the three-interferer and fifteen-interferer cases considered, the SGLM meets or exceeds the performance of the soft-limiting detector and the conventional detector.

We note that (24) can be multiplied by $1/m$ to obtain

$$\tilde{g}_{\text{SGLM}}(x) = \left|\frac{x}{2} + \frac{A_c}{2m}\right| - \left|\frac{x}{2} - \frac{A_c}{2m}\right|. \qquad (25)$$

Comparison of (25) with (18b) reveals that the SGLM can be written in the form of an adaptive soft-limiting detector with threshold $T = A_c/m$. This gives a means of finding an approximate, suboptimal, value of T_{opt} in (18b) without computer search. Specifically, $T_{\text{opt}}/A_c = 1/m$, where m, from (23), is a function of the channel SNR and SIR. The threshold found by this method is not the same as the optimal threshold found by search in [30]; though suboptimal, it may be more convenient since it is expressed in closed-form.

H. P-Order Metric Receiver (p-omr)

The generalized Gaussian distribution has been used to model UWB MUI-plus-noise and applied to UWB receiver design in [34], [35], [37], [38]. The pdf of a random variable X with generalized Gaussian distribution is [56]

$$f_X(x; S_f, \sigma, p) = \frac{1}{2\Gamma(1+1/p)A(p,\sigma)} e^{-\left|\frac{x-S_f}{A(p,\sigma)}\right|^p} \qquad (26)$$

where S_f is a location parameter equal to the mean of X, the function $A(p,\sigma) = \sqrt{\sigma^2\Gamma(1/p)/\Gamma(3/p)}$ is a scale parameter which gives the variance of X as σ^2, and p is a shape parameter. For $p = 2$, the generalized Gaussian distribution becomes the regular Gaussian distribution, while for $p = 1$, the generalized Gaussian distribution becomes the Laplace distribution. The utility of these two special cases in noise modeling and TH-UWB MUI modeling, respectively, suggests that, with suitable choice of p, the generalized Gaussian distribution is a good candidate for modeling the noise-plus-interference in UWB systems.

The optimal receiver is derived in [34], [37], [38]. The structure of the resulting receiver has in common with the other receivers developed thus far that a nonlinear operation is performed on the correlator outputs before summation and decision. The nonlinear operation for the p-omr is given, after normalization, by

$$g_{\text{p-omr}}(x) = \frac{1}{A_c^{p-1}}\left[\left|\frac{x}{2} + \frac{A_c}{2}\right|^p - \left|\frac{x}{2} - \frac{A_c}{2}\right|^p\right]. \qquad (27)$$

In accordance with the properties of the generalized Gaussian distribution, for $p = 2$ the p-omr is the CMF receiver, while for $p = 1$ the p-omr is the soft-limiting receiver. Like the receivers of Sections IV-E through IV-G, the p-omr allows for adaptation between a Laplace-distributed disturbance and a Gaussian-distributed disturbance, and thus provides performance equal to or better than the soft-limiting receiver, and equal to or better than the CMF. A significant difference between the p-omr and the other receivers considered thus far is that the p-omr models MUI *more* impulsive than that modeled by the Laplace distribution and, for some examples, more closely matching the simulated pdf (see Section III and Fig. 5). The shape parameter p provides a means of adaptation to the noise and interference environment, covering from the Gaussian case to the Laplacian case, and beyond. A method to estimate the shape parameter p has been provided in [34], [37] based on the kurtosis of the noise-plus-interference process, discussed in Section VI.

Simulation results shown in [37], [38] for $N_s = 4$ and three interferers (duplicated in Fig. 15) confirm that the p-omr outperforms both the conventional receiver and the soft-limiting receiver, but also show that the p-omr significantly outperforms the adaptive soft-limiting receiver for high SNR. The conventional and soft-limiting receivers show an error floor beyond an SNR of about 20 dB while the p-omr does not show an error floor until about 45 dB; there is no error floor for the p-omr at practical SNRs. This suggests that MUI models that are more impulsive than the Laplace model are appropriate for UWB systems in some channel conditions, and the capability to optimize the parameter p yields a receiver with superior performance.

The p-omr is further extended in [37], [38] to allow an adaptive threshold in (27); i.e.

$$g_{\text{p-omaltr}}(x) = \frac{1}{A_c^{p-1}}\left|\frac{x}{2} + \frac{T_{\text{opt}}}{2}\right|^p - \left|\frac{x}{2} - \frac{T_{\text{opt}}}{2}\right|^p. \qquad (28)$$

This receiver is dubbed the "p-order metric adaptive threshold limiting receiver" (p-omatlr). The BER-optimal threshold T_{opt} is found by computer search after estimation of p by the kurtosis-matching method. It is observed in Fig. 15 that the p-omatlr improves upon the p-omr for SNRs between 18 dB and 35 dB, and the improvement is as much as 2.95 dB.

The parameter p can be found by BER-optimizing computer search instead of kurtosis matching, and the curve of the p-omr receiver with optimized p (but fixed threshold) is also shown in Fig. 15. The performance is observed to be better than the receiver with p found by the kurtosis-matching method, and in addition is observed to be better than the p-omatlr for high SNR. The kurtosis method thus does not find the BER-optimal p. As stated in [37], while the p-omr is based on the generalized Gaussian approximation for the MUI-plus-noise, the actual MUI-plus-noise does not have exactly a

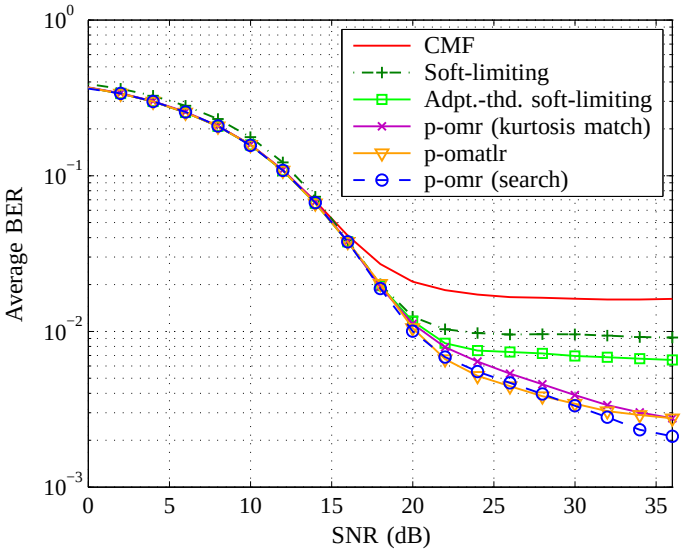

Fig. 15. The average BER versus SNR of the CMF UWB receiver, the soft-limiting UWB receiver, the p-omr with shape parameter determined using the kurtosis matching method and determined by computer search, and the p-omatlr, when both MUI and AWGN are present, and when the SIR is 10 dB (from [37]).

generalized Gaussian distribution, and so an estimator based on this assumption does not provide the optimal value for p.

I. Myriad Filter Receiver

Modeling MUI by a symmetric alpha-stable (SαS) distribution was discussed in Section III and has been applied to UWB receiver designs in [31] and [53].

The characteristic function of an alpha-stable (α-stable) random variable symmetric about μ is

$$\Phi(\omega) = \exp(-\zeta\,|\omega|^{\alpha} + j\omega\mu) \tag{29}$$

where $\zeta > 0$ is called the dispersion, μ is a location parameter, and α is a shape parameter satisfying $0 < \alpha \leq 2$. Alpha-stable distributions have the property that moments greater than α do not exist. Therefore, only the $\alpha = 2$ (Gaussian) case has finite variance.

The problem of optimal detection of a known signal in SαS noise for general α has not been solved. However, a sub-optimal method to estimate the location parameter μ, known as the myriad filter [71], has received attention in recent literature. The moving average myriad filter location estimator is used in [31] to develop an adaptive receiver for detecting UWB signals in the presence of MUI modeled by a symmetric α-stable distribution.

The receiver of [31] can be written in the same form as the other receivers discussed in this paper, that is, as a non-linearity function applied to the partial decision statistics before summation.[3] The receiver in this form is given by

$$\Lambda_{\text{myr}} = \sum_{i=0}^{N_s-1} g_{\text{myr}}(r_i) \tag{30}$$

[3]Note that this is not how the detector is presented in [31]. Putting the detector in the same form, i.e. applying the logarithm, makes the comparison between the various detectors more immediate. However, the form of [31] may be preferred for implementation.

with

$$g_{\text{myr}}(x) = \ln \frac{K^2 + (x + A_c)^2}{K^2 + (x - A_c)^2} \tag{31}$$

and once again the decision statistic Λ_{myr} is compared to a zero threshold to decide the source symbol.[4] The parameter K in the detector is a function of α and adapts the detector to the noise-plus-interference characteristics. The myriad detector becomes the linear CMF detector when $K \to \infty$, is optimal for Cauchy noise when $K = \zeta$, and is optimal in the limit $\alpha \to 0$ when $K = 0$ [71]. An optimal K-versus-α relationship is not known for the full range of α. In [31], K is found using an intuitive formula

$$K^2 = \zeta^{\frac{2}{\alpha}} \left(\frac{\alpha}{2 - \alpha} \right) + C\sigma^2. \tag{32}$$

The first term represents the contribution of MUI to the noise-plus-interference process, while the second term represents the contribution of noise, with C a mixing constant, found experimentally.

The performance of the myriad detector is compared in [31] to the linear CMF receiver, the p-omr with p estimated by kurtosis matching, the SGLM receiver, and a Cauchy detector, for $N_s = 8$ (Fig. 16). It is observed in this example that the myriad detector meets or exceeds the performance of all the other detectors over the entire SNR range. The Cauchy detector is equivalent to a myriad detector with $K = \zeta$, and has been suggested as a good compromise for detection in α-stable noise [72]. The Cauchy detector gives similar performance to the myriad detector for high SNR, but gives inferior performance for low SNR. Thus, the more flexible myriad detector is preferable for UWB applications. At the same time, the excellent performance of the myriad detector for high SNR (i.e., MUI-dominant environments), suggests that the α-stable distribution is an accurate and flexible MUI model. The myriad detector, while suboptimal, is shown to provide superior performance in TH-UWB MUI-plus noise environments.

J. The Zonal UWB Receiver

A novel UWB receiver dubbed the zonal receiver has been investigated in [39], [40]. The basis of the zonal receiver is that in the noise-free case the correlator output amplitude has zones where the sent bit can be distinguished with high reliability, and zones where the sent bit is essentially indistinguishable, and only the former should be considered in the decision statistic.

In the noise-free case, plots of empirical pdfs of the chip correlator output, conditioned on the data bit of the desired user, are provided in [39], [40] and duplicated in Fig. 17. It is observed in [39], [40] that when the data bit 1 is sent, the pdf has an impulse at A_c and a number of other singularities. It is also observed that most of the probability mass is within a region (t_l, t_h), where $t_l < A_c$ and $t_h > A_c$ are the closest singularity points to A_c. The case when the data bit -1 is sent

[4]The function $g_{\text{myr}}(x)$ has been multipled by an additional factor of $A_c/\ln[1 + (2A_c/K)^2]$ for the diagram of Fig. 9. This normalization gives a value of $\pm A_c$ at $x = \pm A_c$, in common with the other detectors.

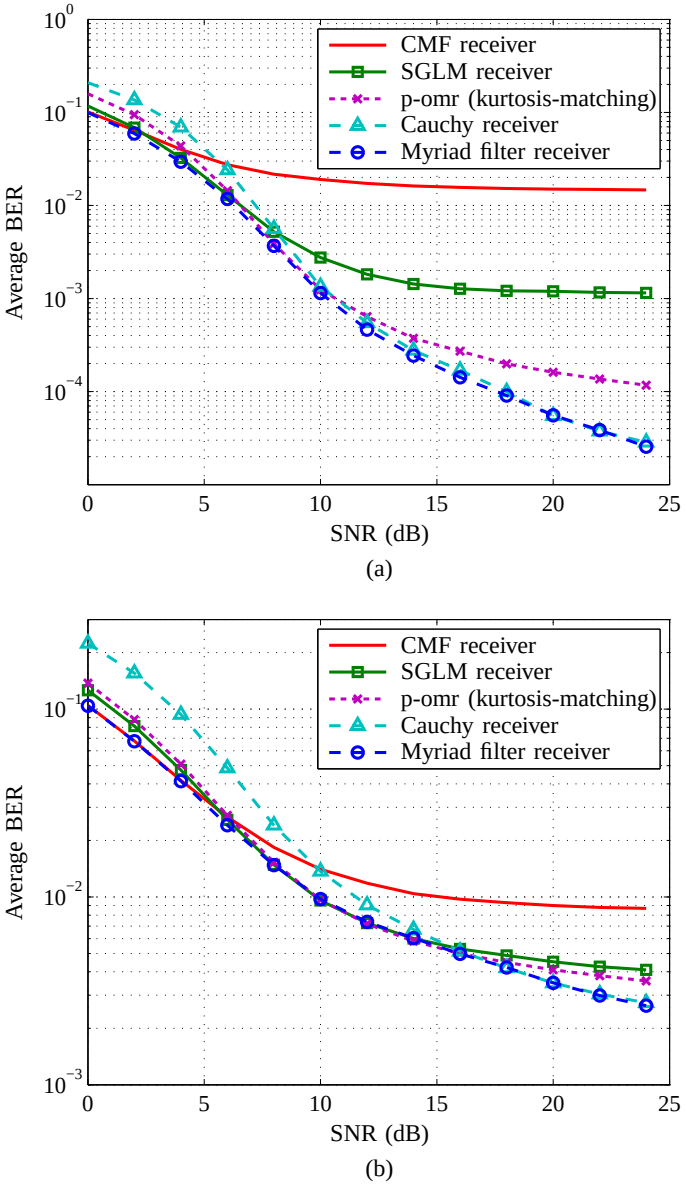

Fig. 16. A comparison of the BER of the myriad detector with the BERs of the linear CMF receiver, the p-omr with p estimated by kurtosis-matching, the SGLM receiver, and the Cauchy receiver, for (a) three interfering users, and (b) fifteen interfering users (from [31]).

is similar, with most of the probability mass in $(-t_h, -t_l)$, $-t_h < -A_c < -t_l$. Considering the two conditional pdfs together, it is observed that outside of these regions the conditional pdfs are of similar and smaller magnitude. Therefore a decision made when $t_l \leq |r_i| \leq t_h$ is much more reliable than a decision made when $|r_i|$ falls outside of this range. Since the contribution of the partial decision statistic r_i is unreliable when $|r_i| < t_l$ or $|r_i| > t_h$, the zonal receiver assigns a weight of zero to any partial decision statistic falling in these ranges. When $t_l \leq |r_i| \leq t_h$, the partial decision statistic contributes r_i to the overall decision statistic. Thus, the zonal receiver forms

$$\Lambda_{\text{zonal}} = \sum_{i=0}^{N_s-1} g_{\text{zonal}}(r_i) \tag{33}$$

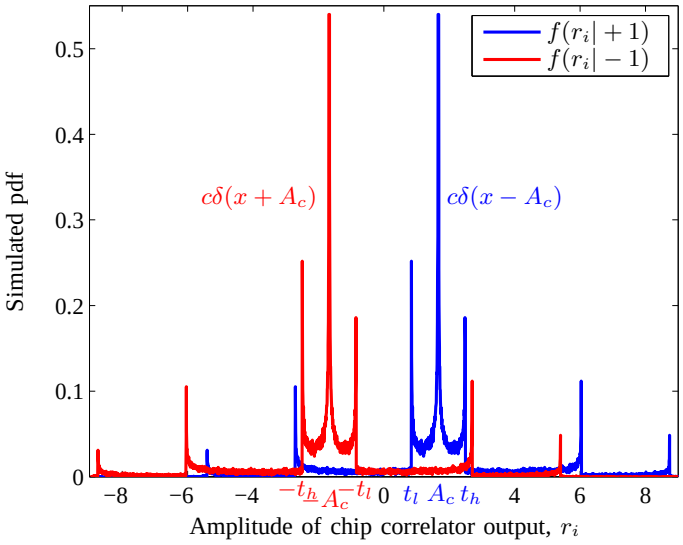

Fig. 17. The simulated conditional pdfs $f(r_i|d_0^{(1)}=+1)$ and $f(r_i|d_0^{(1)}=-1)$ of the amplitude of the chip correlator output $r_i = d_0^{(1)}A_c + I_i$, where I_i is the MUI in the ith frame, the SIR is 10 dB, and c is a constant (from [40]).

where

$$g_{\text{zonal}}(x) = \begin{cases} x & \text{for } x \in (-t_h, -t_l) \text{ or } x \in (t_l, t_h) \\ 0 & \text{otherwise,} \end{cases} \tag{34}$$

and decides on the sent symbol according to

$$\begin{aligned} \Lambda_{\text{zonal}} > 0 &\Longrightarrow d_0^{(1)} = 1 \\ \Lambda_{\text{zonal}} < 0 &\Longrightarrow d_0^{(1)} = -1 \\ \Lambda_{\text{zonal}} = 0 &\Longrightarrow \text{coin toss.} \end{aligned} \tag{35}$$

Effectively, $g_{\text{zonal}}(x)$ forces an erasure of the receiver partial decision statistic whenever a partial decision based on x would be highly unreliable.

The zonal receiver is based on the qualitative nature of the simulated pdf of the chip correlator output r_i; it makes no claims to optimality. In common with the other receivers considered thus far, the CMF UWB receiver is a special case, when $t_l = 0$ and $t_h = \infty$. By optimally adapting t_l and t_h to the channel conditions, the zonal receiver will always meet or outperform the conventional UWB receiver, regardless of noise disturbance. Practical adaptation of t_l and t_h is done by lookup table as described in Section VI.

The BER performance of the zonal receiver is shown in Fig. 18 for $N_s = 4$, together with that of the CMF receiver, the soft-limiting receiver, and the adaptive soft-limiting receiver. The zonal receiver is shown both for SINR estimated using ten symbols, and for perfect knowledge of SNR and SIR. It can be seen that the zonal receiver outperforms the soft-limiting receiver for the full SIR range. For large SNRs, the zonal receiver greatly outperforms the regular and adaptive soft-limiting receivers, and has far better performance than the CMF. Minor performance penalty is reported from using estimated SINR values rather than perfectly known SIR and SNR values. Additional performance results can be found in [39], [40].

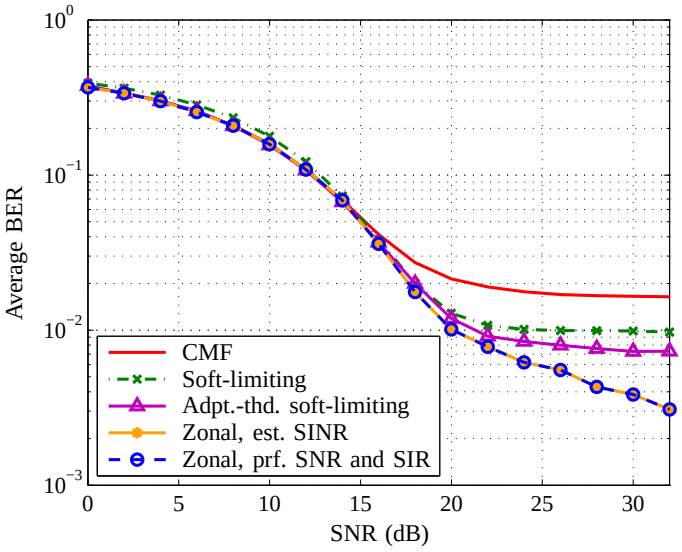

Fig. 18. The average BER versus SNR of the CMF UWB receiver, the soft-limiting UWB receiver, the adaptive threshold soft-limiting UWB receiver, the zonal UWB receiver with thresholds based on the SINR estimated over 10 symbols, and the zonal UWB receiver with thresholds based on perfect knowledge of the SNR and SIR, when both MUI and AWGN are present, and when the SIR is 10 dB (from [40]).

K. The Optimal Performance Benchmark

It is essential to have the optimal performance benchmark against which the performances of other receiver designs can be measured. The ML-optimal detection statistic for the generic receiver structure in Fig. 9 is

$$\Lambda_{\mathrm{ML}} = \sum_{i=0}^{N_s-1} \log \frac{f_{R_i|D}(r_i|d_0^{(1)}=1)}{f_{R_i|D}(r_i|d_0^{(1)}=-1)} \tag{36}$$

and Λ_{ML} is compared with a zero threshold to decide on the source bit. (The ML rule is equivalent to the *maximum a posteriori* rule when the binary source symbols are equiprobable.) The pdf of the MUI for special cases of all the system parameters can be obtained numerically in principle by using extensive simulations assuming sufficient computer resources are available. Similarly, the BER performance of an optimal MUI UWB receiver can be determined for particular cases of system parameters by "brute force" time intensive computer simulations once the "brute force" estimates of the MUI pdfs have been obtained. Results from such an effort have been reported in [70], [73], [74] and are reproduced in Fig. 19. Owing to the onerous time needed to generate these results, statistical variations of the data points are in evidence. Also, some system simplifications were necessary. BER versus SIR curves for the optimal receiver have been computed by simulation for the noise-free case along with those for the p-omr, the soft-limiting receiver, the zonal receiver, the myriad filter receiver, and the CMF. The pulse shape $p_3^e(t)$ of [11] has been employed, with center frequency 6.85 GHz and $T_f = 15$ ns. It can be seen that the p-omr and myriad receivers achieve have similar performance which is very close to the optimal receiver, while the performance of the CMF has almost two orders of magnitude higher BER in some cases. In the case of seven asynchronous interferers, the CMF exhibits

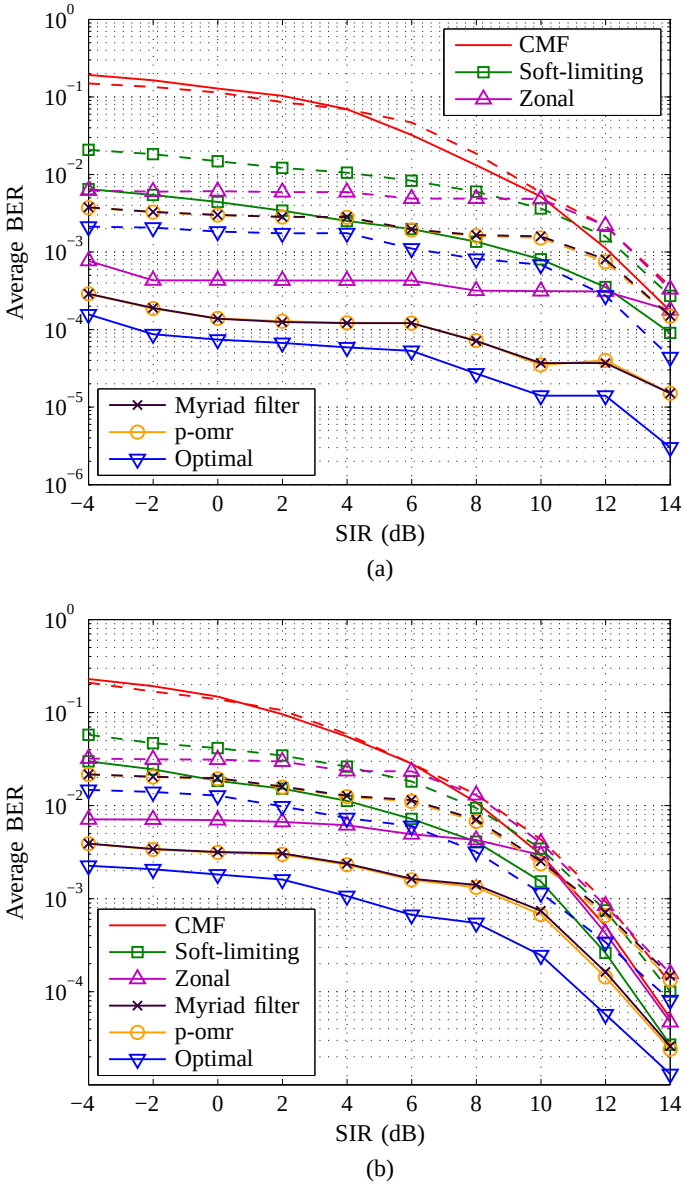

Fig. 19. The BER versus SIR for TH-UWB receivers together with the optimal performance, for (a) seven asynchronous interferers, and (b) fifteen asynchronous interferers (from [74]). Curves for $N_s = 3$ and $N_s = 5$ are depicted by dashed and solid lines, respectively.

significantly higher BERs compared to the optimal receiver, the p-omr, and the myriad filter receiver even for high SIR.

V. Detection in Multipath Fading Channels

The receiver structures and results shown in the previous sections were for a single-path, non-fading channel. Such a channel does not accurately portray typical practical UWB system scenarios, such as indoor applications where multipath is prevalent, so it is imperative to design and analyze useful structures for detection in multipath channels. Two key structures widely studied for UWB systems are the Rake receiver [75] and the autocorrelation receiver with transmitted-reference signaling [76], [77]. The Rake receiver correlates the received signal with signal templates matched to all, or a subset of, the received paths. The outputs of the path correlators

("fingers") are combined in forming a decision on the transmitted symbol, with channel estimation used in forming the correlation templates and in determining combining weights. In transmitted-reference signaling, which is suboptimal but is simpler to implement, an unmodulated reference signal is transmitted along with the modulated information-bearing signal. The reference signal is used as a template for demodulation, with the system designed so that both reference and modulated signals experience the same propagation effects and it is not necessary to estimate individual multipath delays and amplitudes. However, the received reference signal contains noise and interference which degrades performance. The focus of this section is Rake reception of UWB signals, applying the MUI-combatting concepts of Section IV to receiver structures which also combat multipath.

An overview of the UWB multipath channel has been presented in Section II-B. It is characterized by many, perhaps over a hundred, paths between transmitter and receiver, with many paths resolvable at the receiver due to the fine time resolution afforded by the ultra-short UWB pulse. This is in contrast to many narrowband systems, which use a wider signaling pulse and where each resolvable period of delay (delay bin) may have contributions from many multipath components, allowing in some cases for a Central Limit Theorem to provide Gaussian approximations. In a UWB system, the ability to resolve individual multipath components allows for a Rake structure to capture much of the energy in the multipath components and utilize the inherent diversity, at the cost of receiver complexity [75], [78]. Where individual multipath components are resolvable, a Central Limit Theory must be used with caution; it often does not yield accurate approximations.

A Rake receiver consists of a number of fingers, say L. Each finger is matched to a resolvable delay bin or multipath component, and the received signal is passed through all L Rake fingers to provide separate correlator outputs for each delay bin. Rake receivers may be classified as all-Rake, where a Rake finger is matched to each received path; partial-Rake, where a Rake finger is matched to the first L paths; and selection Rake, where a Rake finger is matched to the L strongest paths. In a UWB receiver, each finger performs a partial correlation for each frame; there are $N_s L$ partial correlations across the L fingers and N_s frames are used in the reception of one symbol. Each partial correlation can be written as [19]

$$r_{i,l} = \int_{iT_f + c_i^{(0)} + \kappa_l}^{(i+1)T_f + c_i^{(0)} + \kappa_l} \alpha_l r(t) p(t - iT_f - c_i^{(0)} - \kappa_l) dt \quad (37)$$

where l is the finger index, κ_l is the delay associated with the lth path of the desired user, and α_l is the gain associated with the lth path of the desired user. Analogous to the single-path case, the partial correlations can be written as the sum of a signal part, interference part, and noise part, $r_{i,l} = s_{i,l} + I_{i,l} + N_{i,l}$.

In the conventional Rake receiver the correlator outputs are linearly combined according to some optimal or sub-optimal method, and the combined output is used for signal detection. One such method is maximal ratio combining (MRC), which weights each finger output (or multipath component) according to the ratio between the signal amplitude and the average noise power [79]. Under the assumption of uncorrelated branches (here the fingers are the branches), reference [79] proves that the SNR at the output of the combiner is

$$\rho_{\text{MRC}} = \sum_{l=1}^{L} \rho_l \quad (38)$$

where ρ_l is the SNR on the lth branch. In reference [79] only noise is considered and the term SNR is used to refer precisely to the ratio of signal power to noise power. Importantly, it is readily proved that (38) is valid regardless of the distribution of the noise on each branch and is valid when each branch is subject to the non-Gaussian MUI-plus-noise of a UWB system. Therefore, (38) is valid when $\rho_{\text{MRC,new}}$ and ρ_l are the respective signal–to–MUI-plus-noise ratios of the combiner output and the lth finger, which they shall denote in this paper. Following [30], suppose that the signal–to–MUI-plus-noise ratio in each finger is multiplied by a factor C_l. Then the output signal–to–MUI-plus-noise ratio of the combiner is

$$\rho_{\text{MRC,new}} = \sum_{l=1}^{L} C_l \rho_l. \quad (39)$$

Define $C_{\max}$ and $C_{\min}$ as the maximum and minimum C_l factors, respectively, over the L Rake fingers. The output signal–to–MUI-plus-noise ratio then satisfies

$$C_{\min} \rho_{\text{MRC}} \leq \rho_{\text{MRC,new}} \leq C_{\max} \rho_{\text{MRC}}. \quad (40)$$

The output signal–to–MUI-plus-noise ratio of the MRC Rake combiner is thus determined by $\{C_l\}$, $l = 1, \ldots, L$, where

$$C_l = \frac{\rho_{l,\text{new}}}{\rho_l} \quad (41)$$

and where $\rho_{l,\text{new}}$ is the signal–to–MUI-plus-noise ratio for the lth branch of a novel receiver, and ρ_l is the signal–to–MUI-plus-noise ratio for the lth finger of a conventional Rake receiver containing a CMF in the finger.

Note that when the multipath is dense and the Rake receiver contains a summation over many multipath rays, one might expect the pdf of the output statistic, after combining, to be nearly Gaussian since there is a summation over many multipath components and a Central Limit Theorem may apply. However, in a TH-UWB receiver each Rake finger sees few multipath components and the pdf of the partial decision statistics in each Rake finger output, before summation, is not Gaussian. When the novel receiver structures of Section IV are used in each Rake finger before combining, the output signal–to–MUI-plus-noise ratio of the combiner will be improved, provided $C_{\min} > 1$. Thus, a key property of each of the detection schemes proposed in Section IV versus the linear receiver, in view of the subsequent MRC combining, is enhancement of the output signal–to–MUI-plus-noise ratio per finger.

Accordingly, new Rake receiver designs have been proposed in [19], [37]–[40], [30] applying MUI-suppressing transformations to each Rake finger. A unified block diagram of the proposed Rake structures is given in Fig. 20. In subsequent

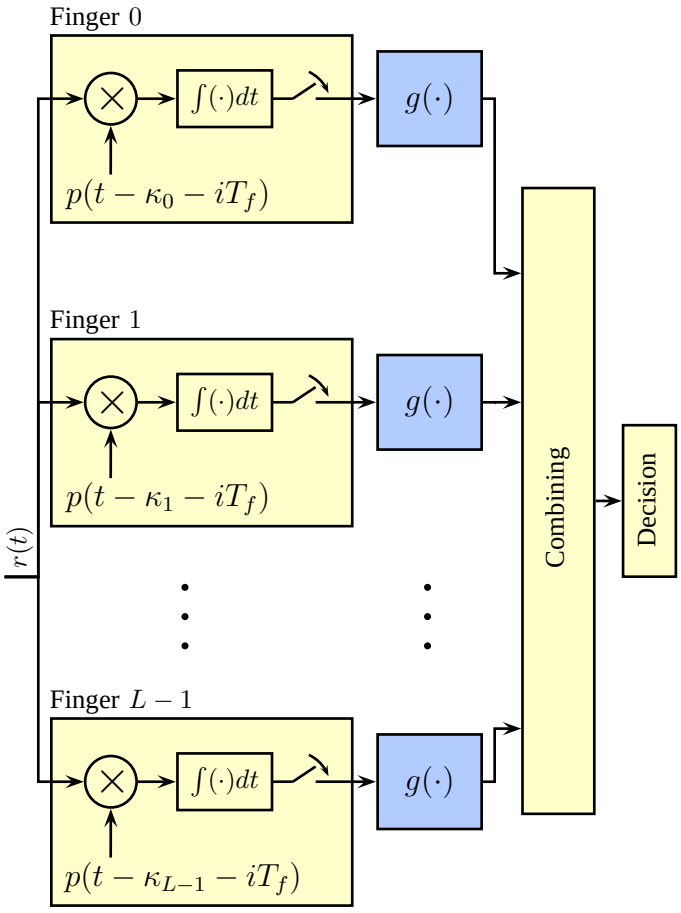

Fig. 20. A unified block diagram of the proposed Rake receiver structures. The nonlinearity functions, applied to each Rake finger, are given in the text.

discussion, we will refer to the signal–to–MUI-plus-noise ratio as the SINR (signal–to–interference-plus-noise ratio), consistent with the references.

A. The Soft-Limiting Rake Receiver

Reference [30] proposes use of the soft-limiting receiver nonlinearity function, or the adaptive soft-limiting receiver nonlinearity, in each finger of a Rake structure before combining. SINR results are presented for the soft-limiting receiver in [30], in comparison with the conventional receiver, and as expected it is found that the SINR per branch is greater for the soft-limiting receiver (i.e., $C_l > 1$) in SNR regions where the BER would be improved in a single-path channel (see Fig. 11). Thus, the overall Rake output SINR, from (40), will also see improvement over these SNR regions.

B. The SGLM-Rake Receiver

The SGLM receiver of Section IV-G is applied to Rake receiver design in [19]. The simplified Gaussian-Laplace mixture receiver is chosen over the optimal GLM receiver as the basis for a Rake design because of the relative complexity and close performance of the two receivers. The GLM receiver, posed for single-path channels as an ML-optimal detection method, is reposed in [19] as a MUI-suppressing nonlinear filtering operation applied to the correlator outputs. Motivated by the effectiveness of the SGLM filtering in suppressing MUI in the single-path case, the nonlinear filtering is applied to the partial correlations of each Rake finger before combining. The assumption is made that the interference terms $I_{i,l}$ are independent and Laplace-distributed when conditioned on the path gains of all users, and while it is noted in [19] that neither assumption is rigorously correct, simulation results support the assumed distribution on $I_{i,l}$ and the performance of the resulting receiver justifies the utility of these assumptions. To further reduce implementation complexity, the variance of the interference in each frame of each finger, which depends on the channel realization, is replaced with its average value and the parameter c redefined accordingly. This average value of c is used for all fingers; however, each SGLM-Rake finger uses a different nonlinearity function according to the path gain. The SGLM is then given by [19][5]

$$\Lambda_{\text{SGLM-SRake}} = \sum_{l=0}^{L-1}\sum_{i=0}^{N_s-1}\left|\frac{m_l r_{i,l}}{2}+\frac{|\alpha_l|\,A_c}{2}\right|-\left|\frac{m_l r_{i,l}}{2}-\frac{|\alpha_l|\,A_c}{2}\right| \quad (42)$$

where

$$m_l = \frac{1-\exp\left(\frac{2|\alpha_l|A_c}{c}\right)\frac{Q(|\alpha_l|A_c/\sigma_n+\sigma_n/c)}{Q(-|\alpha_l|A_c/\sigma_n+\sigma_n/c)}}{1+\exp\left(\frac{2|\alpha_l|A_c}{c}\right)\frac{Q(|\alpha_l|A_c/\sigma_n+\sigma_n/c)}{Q(-|\alpha_l|A_c/\sigma_n+\sigma_n/c)}}. \quad (43)$$

The receiver of [19] is a selection Rake implementation. Note that the SGLM nonlinearity function is applied to the partial decision statistics in each Rake finger before summation.

Performance results are given for the SGLM-Rake receiver in [19], evaluated by simulation for the CM1 channel model [13] with 20 paths per user per realization, equal received power for all users, and $N_s = 8$. The BER performance of the SGLM-Rake receiver is compared to that of the conventional Rake receiver in Fig. 21(a), as a function of SNR for different numbers of interferers. The new receiver is seen to outperform the conventional receiver for larger SNRs and a small to moderate number of interferers, and to match the performance of the conventional receiver for the small SNR region. The diminishing performance gain of the SGLM-Rake as the number of interfering users grows is attributed to the convergence of the interference process to a Gaussian process. The performance comparison is plotted for different numbers of Rake fingers in Fig. 21(b), and it is observed in [19] that the performance improvement is realized regardless of the number of Rake fingers. Since each Rake finger incorporates the SGLM transformation, the MUI-suppression benefits are achieved despite the approach of the interference term in the overall decision statistic to a Gaussian random variable with increasing L.

C. The P-Order Metric Rake Receiver

Reference [37], [38] applies the p-omr to each Rake finger, similarly to the approach described in detail for the SGLM-Rake receiver. The finger outputs are combined using MRC.

[5] A normalizing factor of $c/2$, not found in [19], has been applied to $\Lambda_{\text{SGLM-SRake}}$.

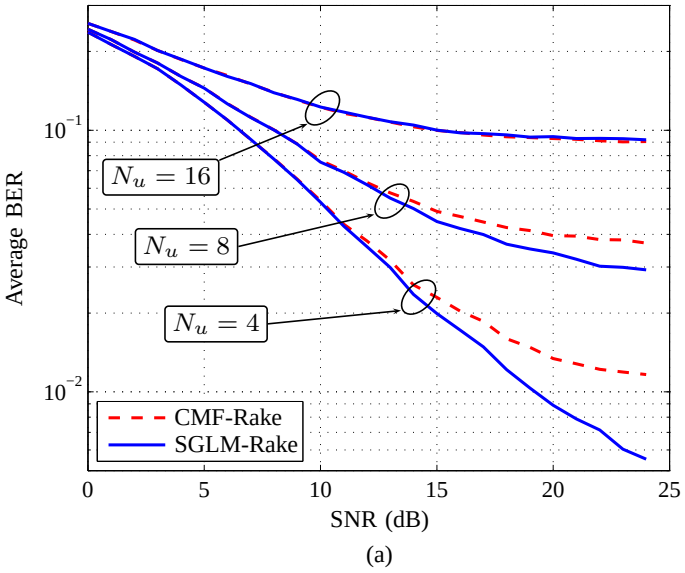

(a)

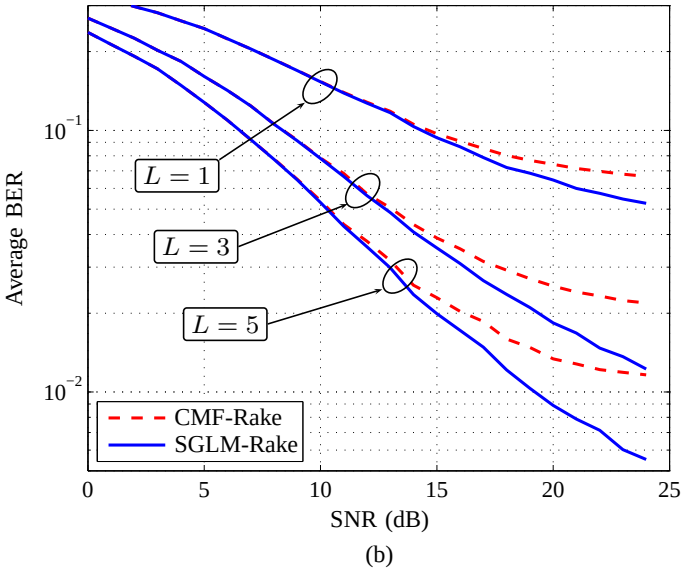

(b)

Fig. 21. A comparison of the BERs of the conventional Rake receiver and the SGLM-Rake receiver for (a) different numbers of equal-power interferers, (b) different numbers of Rake fingers with $N_u = 4$ (from [19]).

In evaluation of the performance of the p-omr Rake receiver, first considered is the illustrative case where the interference-plus-noise disturbance on the lth Rake finger is well-modeled by the generalized Gaussian distribution with $p = 1$, i.e. the Laplace distribution. The corresponding p-omr transformation is used in the lth finger before combining. The SINR of each Rake finger in the new receiver is analytically found to be between two times (for small SINR) and $8/3$ times (for large SINR) the SINR of the conventional Rake receiver. Thus, the SINR of the MRC output can be bounded as in (40) with $C_{\min} = 2 = 3$ dB and $C_{\max} = 8/3 = 4.26$ dB. Values of p other than $p = 1$ have been investigated in [37] numerically (Fig. 22), by comparing input and output SINRs for the p-omr receiver with a simulated interference process of three interferers, for p in (27) equal to 0.2, 0.5, 1.0, 1.5, and 2.0. For this simulated MUI process, the SINR gains are largest

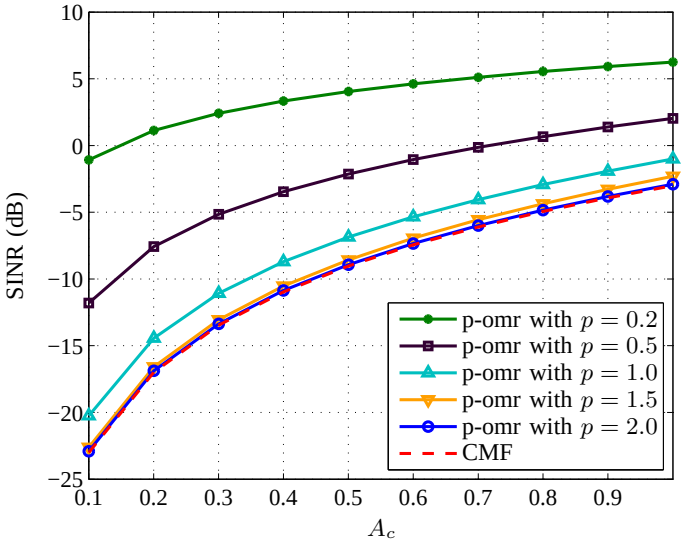

Fig. 22. Comparison between the SINR in each finger of the CMF based Rake receiver and the p-omr Rake receiver, when the shape parameter p assumes different values. A factor N_s not affecting the comparison has been omitted (from [37]).

when p is small, and decrease as p approaches 2, being nil when $p = 2$ since the receiver is exactly the conventional receiver. Thus, a clear benefit in SINR is realized by adopting the p-omr or p-omatlr in the fingers of a Rake receiver in certain SIR/SNR conditions while, with appropriate selection of p, the performance can be no worse than the conventional Rake receiver in any channel conditions.

D. The Zonal-Based Rake Receiver

Use of the zonal receiver in a Rake structure is examined in [39], [40]. A comparison is made between the finger SINR using the conventional correlator and the finger SINR using the zonal receiver transformation, by simulation (see Fig. 23(a)). It is found that the factor $C_{\min} = 1$, while the factor $C_{\max} = 9.3 = 9.7$ dB for a SIR of 5 dB, $C_{\max} = 3.1 = 4.9$ dB for a SIR of 10 dB, and $C_{\max} = 1.4 = 1.6$ dB for a SIR of 15 dB. Since $C_{\min} \geq 1$, the zonal-based Rake receiver performs at least as well as the conventional receiver, and it is superior in channels with strong MUI. This is confirmed in BER simulation results. Fig. 23(b) shows the average BER versus SNR of the zonal Rake receiver and the conventional Rake receiver for several Rake sizes and a SIR of 10 dB, in CM1 channels, with $N_s = 4$. A partial-Rake structure is considered. In this plot the SNR for all curves is determined employing an average signal power using $L = 20$ paths, averaged over many channel realizations. The zonal Rake receiver is seen to have superior performance to the CMF Rake receiver over the range of SNR considered and for each Rake length. Additional BER results can be found in [39], [40] with similar conclusions.

E. The BER-Optimal Linear Rake Receiver for Detection in Symmetric Alpha-Stable Noise

In some cases a linear detector may be desireable for implementation reasons, and the utility of the α-stable model in the nonlinear receiver structure of Section IV-I motivates

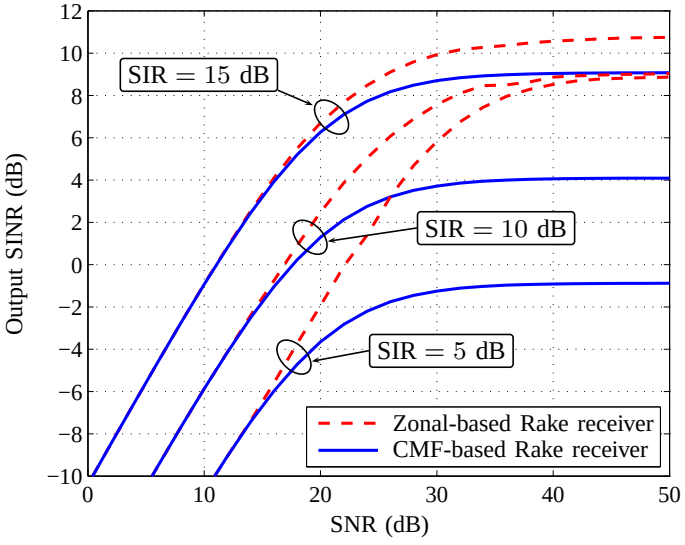

(a)

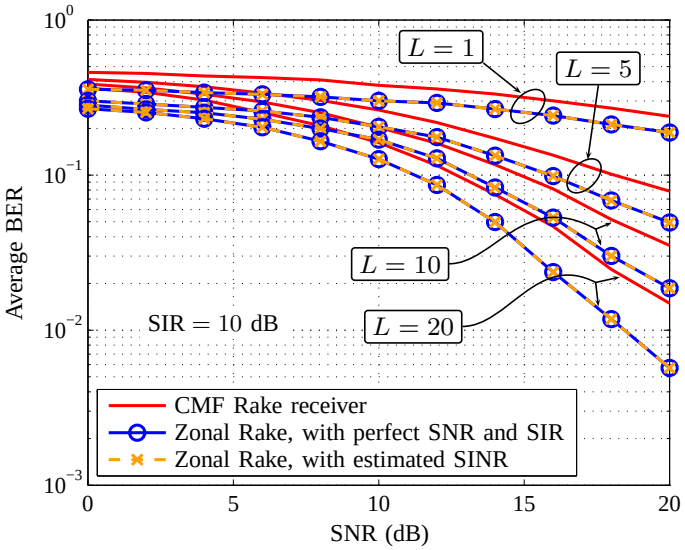

(b)

Fig. 23. (a) The output SINR of the conventional UWB receiver and the zonal UWB receiver with near-optimal thresholds; (b) the average BER versus SNR of the CMF-based Rake receiver, the zonal-based Rake receiver with thresholds based on the estimated SINR, and the zonal-based Rake receiver with thresholds based on perfect knowledge of the SNR and SIR, in CM1 channels, when the SIR is 10 dB (from [40]).

considering whether benefits can be obtained using a linear structure that assumes this MUI-plus-noise model. The receiver considered in this section is the only linear receiver discussed in this paper other than the conventional receiver. The other proposed receivers apply a nonlinear operation to each frame correlator output before combining the partial decision statistics in each Rake finger. The receiver of this section applies no transformation to the frame correlator outputs, but rather obtains weights for *linear* combining of the Rake finger outputs that minimize the probability of bit error when the noise-plus-interference is an α-stable process. Such a detector cannot exceed the performance of a general optimal detector not constrained to be linear, but a BER-optimal linear detector provides a benchmark detector by which to judge nonlinear detection schemes such as those proposed elsewhere in this article.

The novel BER-optimal Rake receiver for detection in symmetric α-stable noise was derived in [53], [54], without restriction to UWB applications. This Rake receiver could be applied to detection of TH-UWB signals. Under the assumption that the partial decision statistics in one Rake finger are jointly α-stable, the Rake finger output formed as a linear combination of the N_s partial decision statistics will also be α-stable [61, Theorem 2.1.2]. Further assuming that the interference-plus-noise processes in the Rake fingers are independent, the weights in [53] are optimal combining weights for the Rake finger outputs. The finger outputs $\{r_l\}_{l=1}^{L}$ are weighted by $\{w_l\}_{l=1}^{L}$ to form the linear Rake combiner output

$$\gamma = \sum_{l=0}^{L-1} w_l r_l \tag{44}$$

and the optimal combining weights $\{w_l\}$ are determined in [54] to be

$$w_l = \text{sign}(s_l)\,|s_l|^{1/(\alpha-1)} \tag{45}$$

where $\{s_l\}$ is the signal component of the finger output.

The advantage of the optimal α-stable combining weights over MRC and equal-gain combining (EGC) have been examined in [53], [54] for signals embedded in ideal α-stable noise with values of the characteristic exponent α from $1 \leq \alpha \leq 2$. A signal-to-noise[6] ratio comparison is maximized over the signal set $\{s_i\}$ to find the maximum SNR advantage of the new combiner over MRC and EGC. This maximum SNR advantage is shown to be very significant, up to approximately 4 dB over MRC for the parameters considered. The advantage is shown to be greater for a larger number of Rake fingers, and to be greatest for small values of α. As α approaches 2, the advantage of the new combiner over MRC approaches zero, since $\alpha = 2$ is the Gaussian case. BER results for 8 Rake fingers and $\alpha = 1.1$ show the SNR advantage of the new combining weights to be approximately 3 dB over MRC and 5 dB over EGC for detection in α-stable noise.

However, preliminary results suggest that the advantages of this linear Rake receiver observed for signals in ideal α-stable noise may not be attained for realistic TH-UWB systems, and that caution must be used when applying interference models to receiver structures. The α-stable model is based on long-term averages of the interference process, while the instantaneous interference for a particular frame in a particular finger is dependent on the time-hopping codes and duty cycle of all users. Each finger in the linear receiver functions as a CMF, and large interference bursts in a single frame corrupt the entire finger output when the frames are linearly combined, leading to poor performance as can be inferred from the results of Section IV. This is in contrast to the proposed nonlinear Rake receivers, where the effect in the finger output of an interference burst in an individual frame is moderated by the nonlinearity function. While the nonlinear receiver of Section IV-I based on the α-stable model is among the best of the receivers considered, the α-stable-optimal linear Rake

[6]In this section, "noise" refers to α-stable noise, not AWGN.

combining considered in this section does not appear to offer a worthwhile advantage over conventional MRC combining for this TH-UWB application.

VI. Estimation of Parameters Required in the New Receiver Structures

Each novel receiver design involves certain parameters that must be adapted or determined from the UWB system design parameters and the channel conditions at the moment of operation. We have deferred discussion of estimation of these parameters until this section in order to streamline the presentation of the various novel receivers. However, practical receivers do not know all system and channel information *a priori*, and thus it is critical to examine the information each receiver requires to operate, and practical estimation methods.

The conventional receiver is the benchmark receiver for both complexity and performance. The conventional receiver operating in an AWGN single-path channel does not require channel state information. However, the conventional Rake receiver used for multipath channels does require channel gain and channel delay information for the desired user in order to usefully combine the output of the Rake fingers, as noted in [30]. It is therefore fair to assume that such information is available to the novel receivers, and examine the additional information required in each receiver design beyond that required by the conventional Rake receiver.

A. The Soft-Limiting Receiver

The soft-limiting receiver of Section IV-D requires the parameter A_c and in turn the channel gain for the desired user, A_1. Since a conventional Rake receiver must estimate A_1, there is effectively no additional channel information required.

B. The Adaptive Soft-Limiting Receiver

The soft-limiting receiver with adaptive threshold requires the optimal value of the threshold, T_{opt}, and the method of [30] is to use a lookup table where the near-optimal threshold is a function of SNR and SIR, and scaled by A_c. Thus, the noise power and interference power must be estimated. Specific methods are neither specified nor evaluated in [30]; SINR estimation methods are found in [80]–[82] and can be utilized with the adaptive soft-limiting receiver. Under a Laplace model for the interference process and the AWGN model, the methods of [19] are appropriate to determine SIR and SNR, as described in the following section.

C. The Gaussian-Laplacian Mixture Receiver

Novel moment-based estimators are proposed in [19] to estimate the parameters σ_n and c required by the GLM and SGLM receivers. The estimators assume that N_T pilot symbols are transmitted, $\{d_b\}_{b=0}^{N_T-1}$, and that the receiver uses a normalized template signal to perform the correlation operation. In a Rake receiver, the estimation is performed in one of the Rake fingers l', forming partial correlations $\{r_{i,b,l'}\}$,

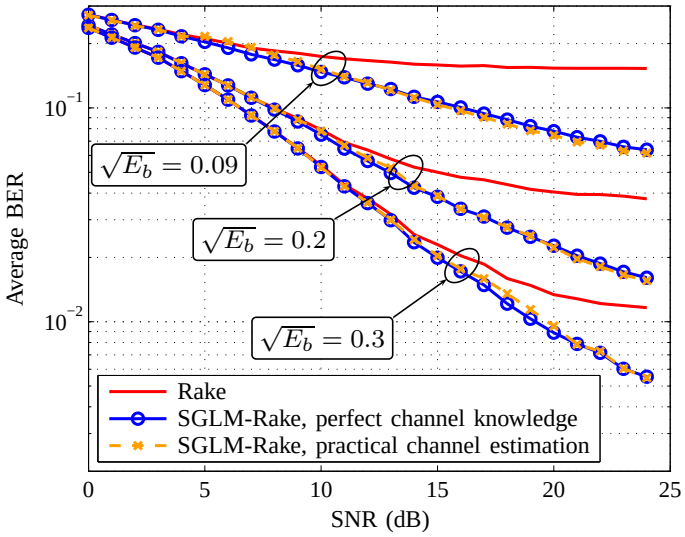

Fig. 24. The BERs of the conventional Rake receiver, the SGLM-Rake receiver with perfect channel knowledge, and the SGLM-Rake receiver with proposed practical channel estimation, for different SIR levels with $N_u = 4$ (from [19]).

$i = 0, \ldots, N_s - 1$. (The non-Rake receiver can be thought of as a Rake structure with one finger.) The estimators are $A_c \approx e_1$,

$$\sigma_n \approx \sqrt{e_2 - 2[(e_4 - 3e_2^2)/12]^{1/2}} \tag{46}$$

and

$$c \approx [(e_4 - 3e_2^2)/12]^{1/4} \tag{47}$$

where $e_1 = (N_s N_T)^{-1} \sum_{b=0}^{N_T-1} \sum_{i=0}^{N_s-1} d_b r_{i,b,l'}$, $e_2 = (N_s N_T)^{-1} \sum_{b=0}^{N_T-1} \sum_{i=0}^{N_s-1} (d_b r_{i,b,l'} - e_1)^2$, and $e_4 = (N_s N_T)^{-1} \sum_{b=0}^{N_T-1} \sum_{i=0}^{N_s-1} (d_b r_{i,b,l'} - e_1)^4$. Derivation of these estimators is given in [19].

Simulation results evaluating the performance of the estimators are given in [19], with $N_s = 8$. The BER performance of the SGLM Rake receiver using perfect channel knowledge is compared with that of the receiver using the practical estimators (46) and (47), and $N_T = 1000$ (Fig. 24). The SGLM receiver is shown to perform very well using the proposed estimators, with performance very close to the perfect-channel-knowledge case.

Recalling that $\boldsymbol{E}\{I_{i,l}^2\} = 2c^2$ for the Rake receiver and $\boldsymbol{E}\{I_i^2\} = 2c^2$ for the non-Rake receiver, these estimators can be used to determine SIR and SNR for other receiver structures. That is, the estimators derived using the GLM model may be useful for SNR and SIR estimation in receiver structures not utilizing this interference-plus-noise model.

D. P-Order Metric Receiver

The p-omr requires estimation of the parameter p, as well as A_c. A method is provided in [34], [37] to form an estimate of p based on the estimated kurtosis of the received signal. It uses the fact that the generalized-Gaussian distribution has zero-valued odd central moments and even central moments which are a known function of p. The value of p is related

to the excess kurtosis of the noise-plus-interference (eq. (5)) according to

$$\varrho(r_i) = \frac{\boldsymbol{E}\{Y_i^4\}}{\boldsymbol{E}^2\{Y_i^2\}} - 3 = \frac{\Gamma(1/p)\Gamma(5/p)}{\Gamma^2(3/p)} - 3. \qquad (48)$$

The value of p can, in turn, be related to the second and fourth moments of the interference I_i and the noise N_i. Details are found in [37].

As noted in Section IV-H, the results of Fig. 15 indicate performance of the p-omr using the kurtosis-matching estimates for p, together with performance using BER-optimizing values of p determined by computer search. The kurtosis-matching method yields inferior receiver performance, attributed in [37] to the fact that the method is based on the generalized Gaussian assumption for the MUI-plus-noise, while the actual MUI-plus-noise distribution does not precisely have a generalized Gaussian pdf. The computer search optimizes p to achieve minimum BER without regard to the underlying distribution. Nonetheless, the kurtosis-matching technique achieves good performance in a ready implementation, as seen in Fig. 15.

E. The Myriad Detector

The myriad detector requires estimates of the parameters ζ and α which define the scale and shape, respectively, of the α-stable approximating distribution for the MUI-plus-noise. A method is provided in [31] to estimate these parameters, based on first estimating a sampled empirical characteristic function of the interference $\Phi_I(\boldsymbol{\omega})$, where $\boldsymbol{\omega}$ is a vector of equally spaced sample points, and then determining α and ζ using a least-squares linear fit to $\ln(-\ln(\Phi_I(\boldsymbol{\omega})))$, where $\ln(\cdot)$ is the natural logarithm. Details are provided in [31]. Work on optimizing the parameter C, which was determined experimentally in [31], is ongoing.

The excellent performance results for the myriad detector presented in [31] (Fig. 16) use the estimated values for α and ζ and attest to the quality of the estimation method for these parameters.

F. The Zonal Receiver

The zonal receiver uses a lookup table to determine t_l and t_h from the channel SIR and SNR. The authors of [39], [40] found that, within a typical range for the number of dominant interferers in a UWB system, the near-optimal thresholds are only weakly sensitive to the number of interferers present. The near-optimal thresholds also were found to be only weakly sensitive to errors in SIR and SNR. Both BER-optimal and SINR-optimal criteria for computer search of t_l and t_h are examined in [39], [40]; it is found that each criterion yields roughly the same thresholds, and so the simpler SINR criterion is recommended for implementations of the zonal receiver. A different table of optimal thresholds is used in the case of a multipath fading channel.

In [40] it is assumed that the interferer gains $\{A_k\}$ are known, and thus the SIR is known, and then the SNR is expressed in terms of the channel SINR as $(\text{SNR})^{-1} = (\text{SINR})^{-1} - (\text{SIR})^{-1}$. The channel SINR is found using the estimators provided in [80], in turn giving SNR and allowing use of the lookup table.

For the proposed zonal-based Rake receiver, SINR is similarly determined using the estimators of [80] applied to each Rake finger, and near-optimal t_l and t_h are found for each Rake finger. The results in Figs. 18 and 23(b), and other results found in [40], show the zonal receiver and zonal Rake receiver to achieve visually identical performance using SINR estimates as using perfect channel information, confirming the excellent performance of the estimators in [80].

Estimation of SIR without simplifying assumptions on the distribution of the interference appears to be an open problem. However, determining SIR from estimated channel parameters could be accomplished, under a simplifying Gaussian-Laplacian mixture model, using the estimators of [19], and these SIR estimates applied to the zonal receiver.

VII. CONCLUSION

It has been demonstrated that the Gaussian approximation to MUI in TH-UWB systems is inaccurate. The Laplace distribution, the Gaussian-Laplacian mixture distribution, the generalized Gaussian distribution, the Gaussian mixture model, the Middleton Class-A noise model, and the α-stable distribution have been considered in this paper for modeling MUI or MUI-plus-noise, and results have been presented showing each to be superior to the Gaussian approximation. These alternative distributions are characterized as being more impulsive than the Gaussian distribution, with slower decay of the pdf tails. The mixing ratio of the Gaussian-Laplacian distribution optimizes the pdf to the MUI-plus-noise channel environment, while the shape parameter serves the same purpose for the generalized Gaussian distribution and the α-stable distribution.

A summary of recently-proposed receiver designs based on several of these models was presented; specifically, the soft-limiting receiver, the adaptive soft-limiting receiver, the Gaussian-Laplacian mixture receiver, the simplified Gaussian-Laplacian mixture receiver, the p-order metric receiver, the p-order metric adaptive threshold limiting receiver, and the myriad detector were discussed. In addition, a zonal receiver based on heuristic techniques was presented. Each of these receivers was shown to provide superior performance in environments where MUI is significant. Several of the proposed receivers meet or exceed the performance of the conventional linear detector in all MUI-plus-noise conditions. Performance results for novel receivers were compared to optimal detection results, based on an accurate theoretical model for the interference which fully explains the features of the MUI pdf.

For reception in multipath fading channels, Rake structures utilizing the novel receiver nonlinearities in each Rake finger were presented. It was shown that with maximal ratio combining, the output SINR of the Rake receivers meets or exceeds the output SINR of the conventional Rake receiver, and that the receivers have BER performance superior to the conventional receiver when MUI is a dominant channel impairment.

None of the proposed receivers are optimal for TH-UWB. However, each provides better performance for operation in MUI than the conventional matched filter UWB receiver.

Comparison with an optimal performance benchmark shows the novel receivers, particularly the p-omr and myriad detector, to achieve performance that is close to optimal. Importantly, the additional complexity required for the novel receivers is reasonable for practical implementations.

REFERENCES

[1] *Revision of Part 15 of the Commission's Rules Regarding Ultra-Wideband Transmission Systems*, Federal Communications Commission (FCC), Feb. 2002, FCC 02–48.

[2] C.-C. Chong, F. Watanabe, and H. Inamura, "Potential of UWB technology for the next generation wireless communications," in *Proc. IEEE Int. Symp. Spread Spectrum Techniques and Applicat. (ISSSTA)*, Manaus, Brazil, Aug. 2006, pp. 422–429.

[3] M. Z. Win and R. A. Scholtz, "Ultra-wide bandwidth time-hopping spread-spectrum impulse radio for wireless multiple-access communications," *IEEE Trans. Commun.*, vol. 48, no. 4, pp. 679–689, Apr. 2000.

[4] ——, "Impulse radio: how it works," *IEEE Commun. Lett.*, vol. 2, no. 2, pp. 36–38, Feb. 1998.

[5] R. Scholtz, "Multiple access with time-hopping impulse modulation," in *Proc. IEEE Military Commun. Conf. (MILCOM)*, vol. 2, Boston, MA, Oct. 1993, pp. 447–450.

[6] A. Giorgetti, M. Chiani, and M. Z. Win, "The effect of narrowband interference on wideband wireless communication systems," *IEEE Trans. Commun.*, vol. 53, no. 12, pp. 2139–2149, Dec. 2005.

[7] M. Z. Win, P. C. Pinto, A. Giorgetti, M. Chiani, and L. A. Shepp, "Error performance of ultrawideband systems in a Poisson field of narrowband interferers," in *Spread Spectrum Techniques and Applications, 2006 IEEE Ninth International Symposium on*, 2006, pp. 410–416.

[8] B. Hu and N. C. Beaulieu, "Performance of an ultra-wideband communication system in the presence of narrowband BPSK- and QPSK-modulated OFDM interference," *IEEE Trans. Commun.*, vol. 54, no. 10, pp. 1720–1724, Oct. 2006.

[9] N. Boubaker and K. B. Letaief, "MMSE multipath diversity combining for multi-access TH-UWB in the presence of NBI," *IEEE Trans. Wireless Commun.*, vol. 5, no. 4, pp. 712–719, Apr. 2006.

[10] G. Durisi and S. Benedetto, "Performance evaluation of TH-PPM UWB systems in the presence of multiuser interference," *IEEE Commun. Lett.*, vol. 7, no. 5, pp. 224–226, May 2003.

[11] N. C. Beaulieu and B. Hu, "A pulse design paradigm for ultra-wideband communication systems," *IEEE Trans. Wireless Commun.*, vol. 5, no. 6, pp. 1274–1278, Jun. 2006.

[12] *IEEE standard for information technology - telecommunications and information exchange between systems - local and metropolitan area networks - specific requirements part 15.3: wireless medium access control (MAC) and physical layer (PHY) specifications for high rate wireless personal area networks (WPANs)*, IEEE Std. 802.15.3-2003, 2003.

[13] A. F. Molisch, J. R. Foerster, and M. Pendergrass, "Channel models for ultrawideband personal area networks," *IEEE Wireless Commun. Mag.*, vol. 10, no. 6, pp. 14–21, Dec. 2003.

[14] D. Cassioli, M. Z. Win, and A. F. Molisch, "The ultra-wide bandwidth indoor channel: from statistical model to simulations," *IEEE J. Select. Areas Commun.*, vol. 20, no. 6, pp. 1247–1257, Aug. 2002.

[15] A. F. Molisch, D. Cassioli, C.-C. Chong, S. Emami, A. Fort, B. Kannan, J. Karedal, J. Kunisch, H. G. Schantz, K. Siwiak, and M. Z. Win, "A comprehensive standardized model for ultrawideband propagation channels," *IEEE Trans. Antennas Propagat.*, vol. 54, no. 11, Part 1, pp. 3151–3166, Nov. 2006.

[16] K. Hao and J. A. Gubner, "The distribution of sums of path gains in the IEEE 802.15.3a UWB channel model," *IEEE Trans. Wireless Commun.*, vol. 6, no. 3, pp. 811–816, Jun. 2007.

[17] N. C. Beaulieu and I. Hosseini, "On the PDF of multiple access interference in time-hopping UWB systems," in *Proc. XXIX General Assembly of the Int. Union of Radio Science (URSI)*, Chicago, IL, Aug. 2008, invited paper.

[18] N. C. Beaulieu and S. Niranjayan, "New UWB receiver designs based on a Gaussian-Laplacian noise-plus-MAI model," in *Proc. IEEE Int. Conf. Commun. (ICC)*, Glasgow, Jun. 2007, pp. 4128–4133.

[19] ——, "UWB receiver designs based on a Gaussian-Laplacian noise-plus-MAI model," *IEEE Trans. Commun.*, 2008, submitted for publication.

[20] B. Hu and N. C. Beaulieu, "Exact bit error rate analysis of TH-PPM UWB systems in the presence of multiple-access interference," *IEEE Commun. Lett.*, vol. 7, no. 12, pp. 572–574, Dec. 2003.

[21] ——, "Accurate evaluation of multiple-access performance in TH-PPM and TH-BPSK UWB systems," *IEEE Trans. Commun.*, vol. 52, no. 10, pp. 1758–1766, Oct. 2004.

[22] ——, "Accurate performance evaluation of time-hopping and direct-sequence UWB systems in multi-user interference," *IEEE Trans. Commun.*, vol. 53, no. 6, pp. 1053–1062, Jun. 2005.

[23] S. Niranjayan, A. Nallanathan, and B. Kannan, "Modeling of multiple access interference and BER derivation for TH and DS UWB multiple access systems," *IEEE Trans. Wireless Commun.*, vol. 5, no. 10, pp. 2794–2804, Oct. 2006.

[24] A. Papoulis and S. U. Pillai, *Probability, Random Variables and Stochastic Processes*, 4th ed. Boston: McGraw Hill, 2002.

[25] Y. Dhibi and T. Kaiser, "On the impulsiveness of multiuser interferences in TH-PPM-UWB systems," *IEEE Trans. Signal Processing*, vol. 54, no. 7, pp. 2853–2857, Jul. 2006.

[26] A. R. Forouzan, M. Nasiri-Kenari, and J. A. Salehi, "Performance analysis of time-hopping spread-spectrum multiple-access systems: uncoded and coded schemes," *IEEE Trans. Wireless Commun.*, vol. 1, no. 4, pp. 671–681, Oct. 2002.

[27] G. Durisi and G. Romano, "On the validity of gaussian approximation to characterize the multiuser capacity of UWB TH PPM," in *Proc. IEEE Conf. Ultra Wideband Syst. and Technologies*, Baltimore, MD, May 2002, pp. 157–161.

[28] N. C. Beaulieu and B. Hu, "An adaptive threshold soft-limiting UWB receiver with improved performance in multiuser interference," in *Proc. IEEE Int. Conf. Ultra-Wideband (ICUWB)*, Waltham, MA, Sep. 2006, pp. 405–410.

[29] ——, "A soft-limiting receiver structure for time-hopping UWB in multiple access interference," in *Proc. IEEE Int. Symp. Spread Spectrum Techniques and Applicat. (ISSSTA)*, Manaus, Brazil, Aug. 2006, pp. 417–421.

[30] ——, "Soft-limiting receiver structures for time-hopping UWB in multiple-access interference," *IEEE Trans. Veh. Technol.*, vol. 57, no. 2, pp. 810–818, Mar. 2008.

[31] S. Niranjayan and N. C. Beaulieu, "A myriad filter detector for UWB multiuser communication," in *Proc. IEEE Int. Conf. Commun.*, Beijing, May 2008, pp. 3918–3922.

[32] B. Hu and N. C. Beaulieu, "On characterizing multiple access interference in TH-UWB systems with impulsive noise models," in *Proc. IEEE Radio and Wireless Symp.*, Orlando, FL, Jan. 2008, pp. 879–882.

[33] ——, "On characterizing multiple access interference in TH-UWB systems with impulsive noise models," 2008, submitted for publication.

[34] J. Fiorina, "WLC28-2: A simple IR-UWB receiver adapted to multi-user interferences," in *Proc. IEEE Globecom*, San Francisco, CA, Nov. 2006, pp. 1–4.

[35] ——, "On the benefit of a one-bit sampling receiver and hard decoding in impulse radio ultra wide band communications with multi-user interferences," in *Proc. IEEE Int. Symp. on Personal, Indoor and Mobile Radio Commun. (PIMRC)*, Helsinki, Finland, Sep. 2006.

[36] J. Fiorina and D. Domenicali, "Revisiting TH-IR-UWB performance limits dependency on essential system parameters using the generalized Gaussian approximation," in *Proc. IEEE Int. Conf. Ultra-Wideband (ICUWB)*, Singapore, Sep. 2007, pp. 751–754.

[37] N. C. Beaulieu, H. Shao, and J. Fiorina, "P-order metric UWB receiver structures with superior performance," *IEEE Trans. Commun.*, Oct. 2008, to be published.

[38] H. Shao and N. C. Beaulieu, "Analysis of a novel p-order metric UWB receiver structure with improved performance in multiple access interference," in *Proc. IEEE Globecom*, Washington, DC, Nov. 2007, pp. 4112–4117.

[39] ——, "A novel zonal UWB receiver structure with improved performance in multiple access interference," in *Proc. IEEE Globecom*, Washington, DC, Nov. 2007, pp. 4118–4123.

[40] ——, "A novel zonal UWB receiver with superior performance," *IEEE Trans. Commun.*, 2008, to be published.

[41] H. El Ghannudi, L. Clavier, and P. A. Rolland, "Modeling multiple access interference in ad hoc networks based on IR-UWB signals up-converted to 60 GHz," in *Proc. European Conf. Wireless Technologies*, Munich, Oct. 2007, pp. 106–109.

[42] P. C. Pinto, C.-C. Chong, A. Giorgetti, M. Chiani, and M. Z. Win, "Narrowband communication in a Poisson field of ultrawideband interferers," in *Proc. IEEE Int. Conf. Ultra-Wideband (ICUWB)*, Waltham, MA, Sep. 2006, pp. 387–392.

[43] T. Erseghe, V. Cellini, and G. Dona, "UWB impulse radio receivers derived from a Gaussian mixture interference model," in *Proc. IEEE Int. Conf. Commun. (ICC)*, Glasgow, Jun. 2007, pp. 5757–5762.

[44] V. Cellini and G. Dona, "A novel joint channel and multi-user interference statistics estimator for UWB-IR based on Gaussian mixture model," in *Proc IEEE Int. Conf. Ultra-Wideband (ICUWB)*, Zurich, Sep. 2005, pp. 655–660.

[45] M.-G. Di Benedetto, L. De Nardis, M. Junk, and G. Giancola, "(UWB)2: Uncoordinated, wireless, baseborn medium access for UWB communication networks," *Mobile Networks and Applications*, vol. 10, no. 5, pp. 663–674, Oct. 2005.

[46] M. Sabattini, E. Masry, and L. B. Milstein, "A non-Gaussian approach to the performance analysis of UWB TH-BPPM systems," in *Proc. IEEE Conf. Ultra Wideband Syst. and Technologies (UWBST)*, Reston, VA, Nov. 2003, pp. 52–55.

[47] K. A. Hamdi and X. Gu, "Bit error rate analysis for TH-CDMA/PPM impulse radio networks," in *Proc. IEEE Wireless Commun. and Networking Conf. (WCNC)*, vol. 1, New Orleans, LA, Mar. 2003, pp. 167–172.

[48] ——, "On the validity of the gaussian approximation for performance analysis of TH-CDMA/OOK impulse radio networks," in *Proc. IEEE Veh. Technol. Conf. (VTC Spring)*, vol. 4, Jeju, Korea, Apr. 2003, pp. 2211–2215.

[49] J. Mitra and L. Lampe, "Robust detectors for TH IR-UWB systems with multiuser interference," in *Proc. IEEE Int. Conf. Ultra-Wideband (ICUWB)*, Singapore, Sep. 2007, pp. 745–750.

[50] V. S. Somayazulu, "Multiple access performance in UWB systems using time hopping vs. direct sequence spreading," in *Proc. IEEE Wireless Commun. and Networking Conf. (WCNC)*, vol. 2, Orlando, FL, Mar. 2002, pp. 522–525.

[51] A. Taha and K. M. Chugg, "A theoretical study on the effects of interference UWB multiple access impulse radio," in *Conf. Rec. Thirty-Sixth Asilomar Conf. Signals, Syst. and Comput.*, vol. 1, Pacific Grove, CA, Nov. 2002, pp. 728–732.

[52] L. Zhao and A. M. Haimovich, "The capacity of an UWB multiple-access communications system," in *Proc. IEEE Int. Conf. Commun.*, vol. 3, New York, Apr. 2002, pp. 1964–1968.

[53] S. Niranjayan and N. C. Beaulieu, "The optimal BER rake receiver for alpha-stable noise," in *Proc. IEEE Int. Conf. Commun.*, Beijing, May 2008, pp. 5013–5017.

[54] ——, "BER optimal linear rake receiver for signal detection in symmetric alpha-stable noise," *IEEE Trans. Commun.*, 2007, submitted for publication.

[55] J. G. Proakis, *Digital Communications*, 4th ed. New York: McGraw-Hill, 2001.

[56] S. M. Kay, *Fundamentals of Statistical Signal Processing. Volume II: Detection Theory*. Upper Saddle River, NJ: Prentice Hall, 1998.

[57] M. Schwartz and L. Shaw, *Signal Processing: Discrete Spectral Analysis, Detection, and Estimation*. New York: McGraw-Hill, 1975.

[58] H. Shao and N. C. Beaulieu, "An analytical method for calculating the bit error rate performance of Rake reception in UWB multipath fading channels," in *Proc. IEEE Int. Conf. Commun.*, Beijing, May 2008, pp. 4855–4860.

[59] ——, "An analytical method for calculating the bit error rate performance of Rake reception in UWB multipath fading channels," 2008, submitted for publication.

[60] W. Feller, *An Introduction to Probability Theory and Its Applications*, 2nd ed. New York: Wiley, 1971, vol. II.

[61] G. Samorodnitsky and M. S. Taqqu, *Stable non-Gaussian random processes*. New York: Chapman & Hall, 1994.

[62] C. L. Nikias and M. Shao, *Signal Processing With Alpha-Stable Distributions and Applications*. New York: Wiley, 1995.

[63] A. P. Dempster, N. M. Laird, and D. B. Rubin, "Maximum likelihood from incomplete data via the EM algorithm," *J. Royal Statistical Soc. Series B*, vol. 39, no. 1, pp. 1–38, 1977.

[64] D. Middleton, "Statistical-physical models of electromagnetic interference," *IEEE Trans. Electromagn. Compat.*, vol. EMC-19, no. 3, pp. 106–127, Sep. 1977.

[65] W. Suwansantisuk, M. Z. Win, and L. A. Shepp, "On the performance of wide-bandwidth signal acquisition in dense multipath channels," *IEEE Trans. Veh. Technol.*, vol. 54, no. 5, pp. 1584–1594, May 2005.

[66] W. Suwansantisuk and M. Z. Win, "Multipath aided rapid acquisition: Optimal search strategies," *IEEE Trans. Inform. Theory*, vol. 53, no. 1, pp. 174–193, 2007.

[67] C. Carbonelli and U. Mengali, "Synchronization algorithms for UWB signals," *IEEE Trans. Commun.*, vol. 54, no. 2, pp. 329–338, Feb. 2006.

[68] L. Yang and G. B. Giannakis, "Timing ultra-wideband signals with dirty templates," *IEEE Trans. Commun.*, vol. 53, no. 11, pp. 1952–1963, Nov. 2005.

[69] N. C. Beaulieu and C. Leung, "On the performance of three suboptimum detection schemes for binary signaling," *IEEE Trans. Commun.*, vol. 33, no. 3, pp. 241–245, Mar. 1985.

[70] N. C. Beaulieu, H. Shao, S. Niranjayan, I. Hosseini, and B. Hu, "Designing ultra-wide bandwidth (UWB) receivers for multi-user interference environments," oral presentation, Harvard School of Engineering and Applied Sciences, Cambridge, MA, May 2008.

[71] J. G. Gonzalez and G. R. Arce, "Optimality of the myriad filter in practical impulsive-noise environments," *IEEE Trans. Signal Processing*, vol. 49, no. 2, pp. 438–441, Feb. 2001.

[72] G. A. Tsihrintzis and C. L. Nikias, "Performance of optimum and suboptimum receivers in the presence of impulsive noise modeled as an alpha-stable process," *IEEE Trans. Commun.*, vol. 43, no. 234, pp. 904–914, Feb./Mar./Apr. 1995.

[73] I. Hosseini and N. C. Beaulieu, "Optimal error rate performance of binary TH-UWB receivers in multiuser interference," in *Proc. IEEE Globecom*, New Orleans, LA, Nov. 2008.

[74] ——, "Bit error rate of binary TH-UWB receivers in multiuser interference," *IEEE Trans. Wireless Commun.*, 2008, submitted for publication.

[75] D. Cassioli, M. Z. Win, F. Vatalaro, and A. F. Molisch, "Low complexity rake receivers in ultra-wideband channels," *IEEE Trans. Wireless Commun.*, vol. 6, no. 4, pp. 1265–1275, Apr. 2007.

[76] J. D. Choi and W. E. Stark, "Performance of ultra-wideband communications with suboptimal receivers in multipath channels," *IEEE J. Select. Areas Commun.*, vol. 20, no. 9, pp. 1754–1766, Dec. 2002.

[77] T. Q. S. Quek and M. Z. Win, "Analysis of UWB transmitted-reference communication systems in dense multipath channels," *IEEE J. Select. Areas Commun.*, vol. 23, no. 9, pp. 1863–1874, Sep. 2005.

[78] M. Z. Win and R. A. Scholtz, "On the energy capture of ultrawide bandwidth signals in dense multipath environments," *IEEE Commun. Lett.*, vol. 2, no. 9, pp. 245–247, Sep. 1998.

[79] D. G. Brennan, "Linear diversity combining techniques," *Proc. IRE*, vol. 47, no. 6, pp. 1075–1102, June 1959.

[80] Y. Chen and N. C. Beaulieu, "SNR estimation methods for UWB systems," *IEEE Trans. Wireless Commun.*, vol. 6, no. 10, pp. 3836–3845, Oct. 2007.

[81] S. Im and E. J. Powers, "An algorithm for estimating signal-to-noise ratio of UWB signals," *IEEE Trans. Veh. Technol.*, vol. 54, no. 5, pp. 1905–1908, Sep. 2005.

[82] D. R. Pauluzzi and N. C. Beaulieu, "A comparison of SNR estimation techniques for the AWGN channel," *IEEE Trans. Commun.*, vol. 48, no. 10, pp. 1681–1691, Oct. 2000.